

2005

Distinguishing Sediment Transport Modes to the Outer-Shelf off the Waiapu River, New Zealand

Lisa D. Addington

College of William and Mary - Virginia Institute of Marine Science

Follow this and additional works at: <https://scholarworks.wm.edu/etd>



Part of the [Oceanography Commons](#)

Recommended Citation

Addington, Lisa D., "Distinguishing Sediment Transport Modes to the Outer-Shelf off the Waiapu River, New Zealand" (2005). *Dissertations, Theses, and Masters Projects*. Paper 1539617835.

<https://dx.doi.org/doi:10.25773/v5-rxc9-3w90>

This Thesis is brought to you for free and open access by the Theses, Dissertations, & Master Projects at W&M ScholarWorks. It has been accepted for inclusion in Dissertations, Theses, and Masters Projects by an authorized administrator of W&M ScholarWorks. For more information, please contact scholarworks@wm.edu.

DISTINGUISHING SEDIMENT TRANSPORT MODES TO THE OUTER-SHELF
OFF THE WAIAPU RIVER, NEW ZEALAND

A Thesis

Presented to

The Faculty of the School of Marine Science

The College of William and Mary in Virginia

In Partial Fulfillment

Of the Requirements for the Degree of

Master of Science

by

Lisa D. Addington

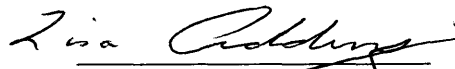
2005

APPROVAL SHEET

This thesis is submitted in partial fulfillment of


The requirements for the degree of

Master of Science

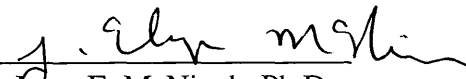


Lisa D. Addington

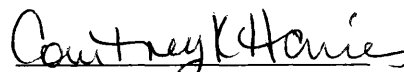
Approved, December 2005



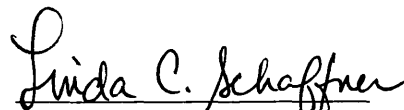
Steven A. Kuehl, Ph.D.
Committee Chairman/Advisor



Jesse E. McNinch, Ph.D.



Courtney K. Harris, Ph.D.



Linda C. Schaffner, Ph.D.

TABLE OF CONTENTS

	Page
ACKNOWLEDGMENTS.	v
LIST OF TABLES.	vi
LIST OF FIGURES.	vii
ABSTRACT.	viii
INTRODUCTION.	2
BACKGROUND.	5
Geological and Oceanographic Setting.	5
Transport Mechanisms.	8
River Inflows.	8
Gravity Dominated Flows.	10
Hyperpycnal Flows.	10
Bottom- Boundary Layer Transport.	11
Use of Sediment Geochronology in Shelf Studies.	12
METHODS.	13
Sonar Equipment and Data Processing.	13
Survey and Sampling.	14
Laboratory Techniques.	16
RESULTS.	18
Shelf-edge Morphology.	18
Sub-bottom features.	20
Pb-210.	28
X-radiograph images.	29

Grain Size.	32
⁷ Be distribution.	36
Carbon.	38
DISCUSSION.	40
Stratigraphic Interpretation.	40
Northern Basins.	40
Southern Shelf.	41
Recent Accumulation.	42
Northern Basins.	42
Southern Shelf.	43
Combined Recent Accumulation across the Region.	44
Transport Mechanisms.	44
CONCLUSIONS.	52
APPENDICES.	54
LITERATURE CITED.	60

ACKNOWLEDGMENTS

I greatly appreciate all of those who aided in the successful completion of my master's project. Thanks to my advisor, Dr. Steve Kuehl, not only for providing the opportunity of many wonderful travel experiences, but also for the knowledge, support, and laughter he continuously supplies. I feel very privileged to have had an advisor whose personality meshed so well with mine and consider him a lifelong friend and supplier of chocolate. I also greatly appreciate Dr. Jesse McNinch for adopting me as a pseudo-pelican and allowing me to expand the knowledge and resources available for my use in executing my project. Thanks to Dr. Courtney Harris and Dr. Linda Schaffner, both highly appreciated committee members who always managed to provide insight from different angles, helping to add dimension to my thesis. My lab members have also been very supportive over the years and provided input on ideas along with moral support as well as helping with my laboratory work. I would like to thank the crew of the RV Kilo Moana, the kiwis from NIWA and GNS, members of the VIMS community, and the W&M undergraduates who aided in the collection of the samples used for my project. Many thanks go to all of my VIMS friends. I could have never expected meeting such an excellent group of people who have made my time here so enjoyable. Thanks also to Eddie for the support, which was appreciated despite it being primarily through long-distance calls. Last, but certainly not least is the great appreciation that I have for my wonderful family who have all loved, sacrificed, supported, and encouraged me in all my endeavors.

LIST OF TABLES

Table	Page
Table 1: Grain size calculations within ^{210}Pb supported region	35
Table 2: ^7Be activities for box cores.	37

LIST OF FIGURES

Figure	Page
Fig. 1: Map of Waiapu Shelf with study site.	7
Fig. 2: Map with transect and core locations.	15
Fig. 3: Multibeam bathymetric image of study site.	19
Fig. 4A: Chirp Sub-bottom profile of Transect 1 with core locations.	21
Fig. 4B: ^{210}Pb profiles along transect 1.	21
Fig. 5A: Chirp Sub-bottom profile of Transect 2 with core locations.	23
Fig. 5B: ^{210}Pb profiles along transect 2.	23
Fig. 6A: Chirp Sub-bottom profile of Transect 3 with core locations.	25
Fig. 6B: ^{210}Pb profiles along transect 3.	25
Fig. 7A: Chirp Sub-bottom profile of Transect 4 with core locations.	27
Fig. 7B: ^{210}Pb profiles along transect 4.	27
Fig. 8: X-radiograph images from transect 1,3, and 4.	31
Fig. 9: ^{210}Pb profile of KC4C with sand, silt, and clay size-fractions.	33
Fig. 10: Clay normalized excess ^{210}Pb profile.	34
Fig. 11: N/C versus $\text{De}13\text{C}$ along transects 3 and 4.	39
Fig. 12: Inventory versus accumulation rates along the outer-shelf.	45
Fig. 13: Proposed sediment transport pathways.	51

Abstract:

Distinguishing sediment transport modes to the outer-shelf off the Waiapu River, New Zealand

Recent studies on continental margins suggest that small, high-yield rivers are capable of generating frequent hyperpycnal flows, an idea that fundamentally alters our understanding of material flux from the continents to the ocean. Formation of negatively buoyant flows is generally considered to occur when suspended sediment concentrations exceed 36 kg m^{-3} (Mulder et al., 2003). Discharge measurements indicate that the Waiapu River, North Island, New Zealand surpasses this value on a yearly basis. Additionally, continental shelves with high wave activity are often capable of producing high density flows within the bottom boundary layer as a result of sediment resuspension (Wright et al., 2001).

This study contrasts shelf-edge basins with relatively flat areas along the shelf-edge, thereby testing the idea that hyperpycnal deposits propagate to topographic lows. Observations and measurements through geochemical and sedimentological analyses of sediment cores, EM1002 swath, and Chirp sub-bottom profiles suggest differing transport modalities on the outer shelf. In general the southern flat region exhibits high terrigenous inputs and non-steady state ^{210}Pb profiles, whereas the northern basin area contains steady-state ^{210}Pb profiles and increased marine influence. High-density flows dominate accumulation in the southern region, whereas within the northern portion, surface plume sedimentation is indicated. Overall this study suggests that high-density flows could be bypassing the northern basins, perhaps a result of oceanographic influences and bathymetric steering as they seek a more direct route across the shelf.

DISTINGUISHING SEDIMENT TRANSPORT MODES TO THE OUTER-SHELF OFF THE WAIAPU RIVER, NEW ZEALAND

INTRODUCTION

Rivers with the highest sediment yields frequently coincide with areas of intense tectonic activity (Milliman and Syvitski, 1992). Small rivers, specifically those located in southern Asia and islands of the Western Pacific, compose a large percentage (~70%) of global sediment discharge (Milliman and Meade, 1983). These small rivers in tectonically active locations show significant inter-annual variation in sediment discharge, making it difficult to accurately portray the impacts of major events that may play a major role in sediment delivery to the world ocean (Farnsworth and Milliman, 2003).

The Waiapu River drains a small watershed (1734 km²) along the mountainous and tectonically active north-east region of the North Island, New Zealand. Geomorphic conditions, coupled with high annual rainfall and the effects of deforestation, produce high concentrations of sediment in the local rivers. A sediment yield of 20,520 t km⁻² yr⁻¹ has been calculated for the Waiapu River (Hicks et al., 2003), one of the highest in the world. A significant amount of this sediment potentially escapes to the outer shelf and beyond, in part because of the narrow continental shelf, typical of active margins (Farnsworth and Milliman, 2003). However, the mechanisms of across-shelf transport are not fully understood.

There are four primary transport methods capable of carrying riverine material to the outer shelf. River flow can form surface plumes and deposition along the shelf

occurs as sediment settles from the plume. Downwelling of the river plume can result in suspended sediment trapping within the bottom boundary layer, which can then be transported offshore within the near-bed region (Davies and Xing, 2002).

Alternatively, hyperpycnal inflows may be formed at the mouth of the Waiapu during seasonal floods and advect sediment across the shelf under the influence of gravity.

High-density flows can also be created within the bottom-boundary layer where a critical concentration of sediment is reached, which acts to decrease the extent of resuspension, causing a thin fluid mud layer to propagate as a gravity-driven flow (Scully et al., 2002). It is also possible that some combination of these types of transport may occur.

Hyperpycnal plumes, a phenomenon that until recent years had been thought of as rare in the marine environment, are now considered to occur more frequently off the mouths of small- to medium- sized rivers (Mulder et al., 2003). These flows occur when river discharge has a higher density than the water in the receiving basin. In freshwater lake environments, this higher density can be caused by decreased temperature of river inflow, but in the marine environment, suspended sediment concentrations on the order of 36 kg m^{-3} are necessary to exceed the density of saline waters in the receiving basin (Mulder et al., 2003). Extreme floods with high suspended sediment concentrations are one of the primary conditions that lead to the formation of hyperpycnal flows in marine environments. These flows have been found to play a significant role in transporting sediment offshore of small to medium mountainous rivers. Hyperpycnal inflows may be common off the Waiapu River, where river suspended sediment concentrations of 90 kg l^{-1} have been measured

(Hicks and Griffiths, 1992). Therefore the Waiapu represents a natural laboratory for the study of this important process.

As a result of tectonic activity, the Waiapu continental margin is partitioned into a number of discrete basins, including several shelf-edge basins that constitute our study area. This research addresses the processes by which sediment is transported to the outer shelf, and how the processes vary within and between individual basins. Through targeted coring and acoustic observations of the shelf-edge, differences in patterns of sediment accumulation along the outer shelf as well as within the intra-basin regions will be elucidated. This study contrasts shelf-edge basins with relatively flat areas along the shelf-edge, testing whether there is evidence of different modes of sediment delivery to these areas.

BACKGROUND

Geological and Oceanographic Setting

The east coast of the North Island of New Zealand represents a highly complex tectonic environment, lying on the margins of the Australian and Pacific plates, where the Australian Plate is being obliquely subducted. These conditions have resulted in the formation of a number of different environments including a frontal wedge, a fore-arc basin, and uplifted basement (Walcott, 1987). A large percentage of the Waiapu catchment contains a portion of the East Coast Allochthon (Page et al., 2001). Through tectonic thrusting the sedimentary rocks that dominate this sequence have become crushed, sheared, and thereby more susceptible to erosion.

The upper section of the Waiapu River begins as a single channel, but the river becomes braided within the last 26 km. In the upper reaches the terrain is predominantly sandstone and mudstone, which changes to gravel in the lower segment (Page et al., 2001). The average annual rainfall value for the watershed is 2,400 mm/year with large storms having a recurrence interval between 2.6 and 3.6 years across the reaches of the Waiapu (Hicks, 1995). The Waiapu catchment's composition of mudstone, high rainfall, and land use practices have given rise to the highest sediment discharge in New Zealand, ~ 35 Mt/year (Hicks et al., 2003).

During high flood events, suspended sediment concentrations up to 90,000 mg l⁻¹ have been recorded (Hicks and Griffiths, 1992).

The Waiapu empties out of East Cape onto a narrow shelf characterized by a complex bathymetry. Previous swath bathymetric studies made through the use of an EM300 multi-beam system have revealed the presence of a number of tectonic features on the slope and shelf, including sub-marine canyons, a major debris avalanche deposit (the Ruatoria) (Collot et al., 2001; Lewis and Barnes, 1999; Carter et al., 1996), and a series of outer-shelf basins. These shelf-edge basins, which include one bi-lobed basin measuring approximately 8 km², 1 smaller 4 km² basin slightly to the north-east, as well as a series of shore-parallel plateaus further south, have become the focus of this project.

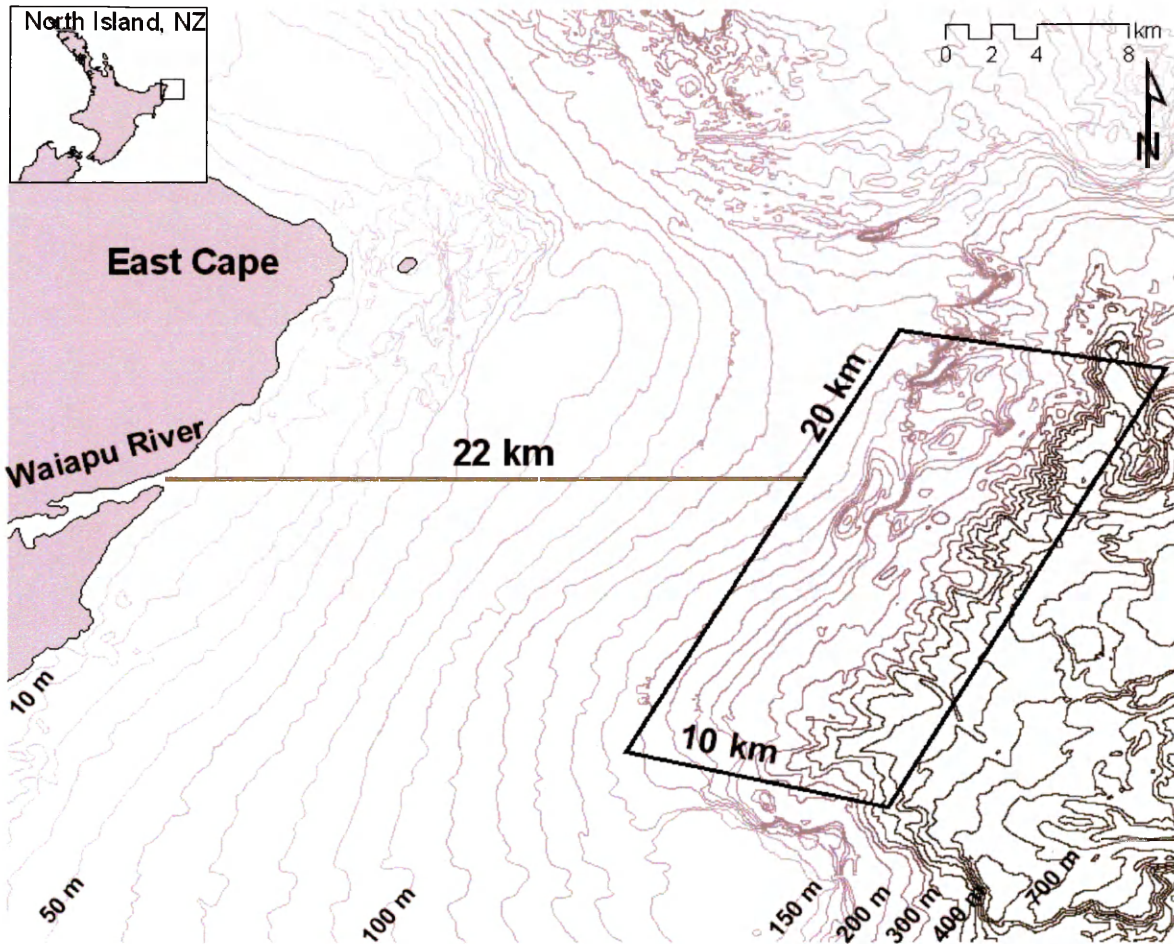


Fig. 1: Shelf off the Waiapu river, with bathymetric lines provided by NIWA. The area within the black square represents the study site, approximately 22 km off the river mouth, spanning an area of 20km x 10km of the outer-shelf.

The east coast of the North Island of New Zealand is influenced by a number of oceanic currents, primarily the East Auckland Current and the East Cape Current, both of which are composed of warm subtropical waters. To the south of East Cape, there exists the northward flowing Wairarapa current, with an influence from the D'Urville Current, the Southland Current, as well as the East Cape Current. The interaction of the East Cape Current with the Wairarapa Coastal current produces the Wairarapa Eddy off the Southeast coast of the North Island (Chiswell, 2000). The East Cape region is dominated by waves moving in a northeasterly direction with heights generally less than 3 meters (Pickrill and Mitchell, 1979). During the active winter-storm season wave heights greater than 10 meters have been recorded (Wright et al., 2005).

Transport Mechanisms

River Inflows

Riverine water entering the coastal environment is strongly influenced by buoyancy. The three types of flows categorized by the density difference between riverine and oceanic water include hypopycnal, homopycnal, and hyperpycnal flows. The simplified model of buoyant plumes entering the marine environment states that it expands as a homogenous layer, thinning vertically with distance from the river mouth, which results in increased mixing and a fining deposit moving seaward (Wright, 1977). More recent studies indicate that the outflow conditions off the river mouth, degree of mixing within the inner shelf, and width of the frontal zone have a

great impact on the river plume and associated sediment. These influencing factors include the inertia of the river outflow, earth's rotation, winds, currents, and particle flocculation (Geyer et al., 2004; Kranck and Milligan, 1991).

Berdeal et al. (2002) examined how regional wind conditions influence both the width and location of the river plume. Upwelling and downwelling currents are created during specific wind-settings and can greatly affect the nature of the river plume. During downwelling conditions, a fast, narrow river plume exists, which can form a coastal current, propagating along-shelf, parallel to the coast. Alternatively, when an upwelling current develops, a much slower, broader plume is produced from which sedimentation occurs over a more dispersed area.

Sediment can become disassociated from the river plume through flocculation of sediment particles within the frontal zone (Geyer et al., 2004). Sediment is primarily trapped in wide frontal zones, present in locations with shallow inner shelves and strong tidal currents. In locations where the river enters into deep surrounding water and is subjected to weaker tidal energy, more narrow frontal zones exist and sediment is more likely to maintain its association with the river plume. The Waiapu river empties out onto a steeply graded slope as a result of the tectonically active East Cape margin. The presence of this steep, shelf indicates that the frontal zone off the Waiapu mouth is likely concentrated and narrow, allowing for the escape of more suspended sediment within the river plume.

Particle disassociation from the river plume often occurs along the inner shelf. Within well-mixed plumes this deposition is only temporary due to resuspension of particles within the energetic nearshore environment, which is the case off the mouth

of the Eel River, California. Resuspended sediments can then recombine with the river plume and continue to be transported through the process of mixing (Geyer et al., 2000).

Gravity dominated flows

For the remainder of this paper, all gravity driven transport will be referred to as density flows. These include hyperpycnal flows as well as wave-driven bottom boundary layer transport.

Hyperpycnal flows- One method of producing gravity-driven flow occurs when high sediment concentrations at river mouths cause the incoming flow to exceed the density of the receiving basin waters, referred to as hyperpycnal flows. Various studies have examined the different mechanisms that are capable of generating this type of transport (e.g., Mulder and Syvitski, 1995; Mulder et al., 1998a; Parsons et al., 2001). Mulder et al. (2003) outline some of these mechanisms in addition to specific environmental conditions that act to decrease the critical concentrations that must be reached in order to form hyperpycnal plumes. In general, conditions that aid in the formation of dense river inflows to the ocean include the presence of easily erodible soil, occurrence of extreme geological events, and decreased river size. The easily erodible mudstone of the east coast of New Zealand, high rainfall, tectonic activity, and small catchment size make the rivers located in this region likely to have a high frequency of hyperpycnal plume formation.

Hyperpycnal flows form specific deposits, hyperpycnites, with variations depending on flow conditions. The general pattern observed is a coarsening-up

deposit formed during the waxing period of the flood overlain by a fining-up deposit formed during the waning phase of the flood (Mulder et al., 2003). There is typically a sharp contrast between these two units, often marked by an erosional surface.

Along with the variation in grain size, these deposits often contain significant inputs of organic matter from land, such as leaves and woody material.

Bottom-boundary layer transport- In addition to hyperpycnal inflows described above, sediment gravity flows on the continental shelf can result from wave-current interaction within the boundary layer and divergence along salinity fronts, among other mechanisms (Traykovski et al., 2000; Wright et al., 2001; Scully et al., 2002, Kineke et al., 2000). During periods of elevated river discharge with increased concentration and high wave-energy, fluid mud layers within the wave boundary can develop and propagate across the shelf as gravity-driven currents (Traykovski et al., 2000). Fluid-mud in the wave boundary layer can only be maintained at depths where the wave-energy is capable of suspending sediment, which is generally considered to be a maximum depth of around 110 m. Strong ambient waves and a sufficient supply of easily suspended sediment are necessary in order to reach and sustain gravity-induced transport (Wright et al., 2001). During periods when greater amounts of sediment are delivered from the river mouth, gravity driven processes dominate due to the critical stratification that occurs within the wave-boundary layer (Scully et al., 2002). The shelf gradient has a direct influence on the strength of this transport process where the probability of strong gravity-induced transport decreases with a decrease in gradient.

Use of Sediment Geochronology in Shelf Studies

Particle reactive radioisotopes are a frequently used tool in the study of marine sediment deposits (e.g., Sommerfield and Nittrouer, 1999; Alexander and Venherm, 2003; Lewis et al., 2002). ^{210}Pb ($t_{1/2}=22.3$ years) is often used in determining accumulation rates on a centennial scale. ^{210}Pb is supplied to the ocean through runoff, atmospheric precipitation, and water-column decay of its parent, ^{226}Ra . The preferential removal of particle-reactive ^{210}Pb causes it to be found in excess in the sediments, where sediment accumulation can be estimated during the time it takes for secular equilibrium to be reached. The use of ^{210}Pb geochronology is most applicable in regions where silt and clay are the dominant grain-sizes, physical and biological reworking are minimal, and accumulation rates exceed 1 mm yr^{-1} (Nittrouer et al., 1979).

In addition to the sediment processes on the 100-year time scale, the capabilities also exist to distinguish deposition during individual seasons. One method used to better understand seasonal sediment deposition is through the use of short-lived radioisotopes, including ^7Be (Giffin & Corbett, 2003). ^7Be ($t_{1/2}=53$ days) is atmospherically derived through nuclear spallation reactions and is deposited to the Earth's surface via wet and dry deposition where it quickly sorbs to inorganic particles. Through inventory calculations within individual box cores, it is possible to use short-lived radioisotopes to trace seasonal flood deposits (Sommerfield et al., 1999; Mullenbach and Nittrouer, 2000).

METHODS

Sonar Equipment and Data Processing

A high-resolution bathymetric map of the shelf and adjacent environments was created in May, 2004 using a ship-mounted Simrad EM1002 multibeam, aboard the *R/V Kilo Moana*. The EM1002 has a frequency of 95 kHz, 111 beams per ping, a maximum ping rate of greater than 10 Hz, and a coverage sector up to 190°. An Edgetech SB-512i (Chirp) was utilized for subbottom profiling, with a frequency range of 500 Hz-12 kHz, a vertical resolution of 8-20 cm, beam width of 16°-32°, a towing speed up to 7 knots, and depth of penetration ranging from 5 to 60 meters depending on the sediment type. The Chirp sub-bottom profile aids in understanding the architecture and mechanism of formation of the shelf-edge features and reveals longer term sedimentation patterns.

Processing of Chirp data was accomplished through the software program SonarWeb. This program allowed for visualization of the profiles, creation of high-resolution images, and digitization of reflectors. Profiles were then exported to the software program Fledermaus, which allowed for the viewing of swath data in conjunction with chirp profiles in order to compare the sub-bottom reflectors with seafloor morphology.

Survey and Sampling

In May 2004, a grid of along and across shelf transects of both the Chirp and EM1002 was run on the outer shelf in the region shown in Figure 2. Cores were collected along chirp survey lines in order to ground-truth the seismic data and for sedimentological and geochemical studies. Cores were collected across the shelf on the basis of bathymetry data; moving offshore the features targeted include: the shelf shoreward of the basin, shoreward basin-edge, basin-low, seaward edge, and seaward plateau for each basin (Fig. 2). Seabed sampling equipment used includes kasten and box corers. Twenty-five kasten cores were collected with lengths ranging from 0-250 cm, processing included the removal of sections for x-radiography as well as sampling discrete intervals for post-cruise laboratory analysis. The sub-cores were x-radiographed on board for sedimentary structure analysis. Box core sites were targeted at the same locations as the kasten cores in order to obtain both 100-year and seasonal data for each site. The box corer allows for the collection of relatively undisturbed surface sediment. Processing is similar to that used for the kasten cores in that it involves the removal of slabs for x-radiography, but before sub-samples can be taken, 6-inch diameter PVC tubes are used to collect sub-cores. An extruder is then used to sub-sample these individual cores.

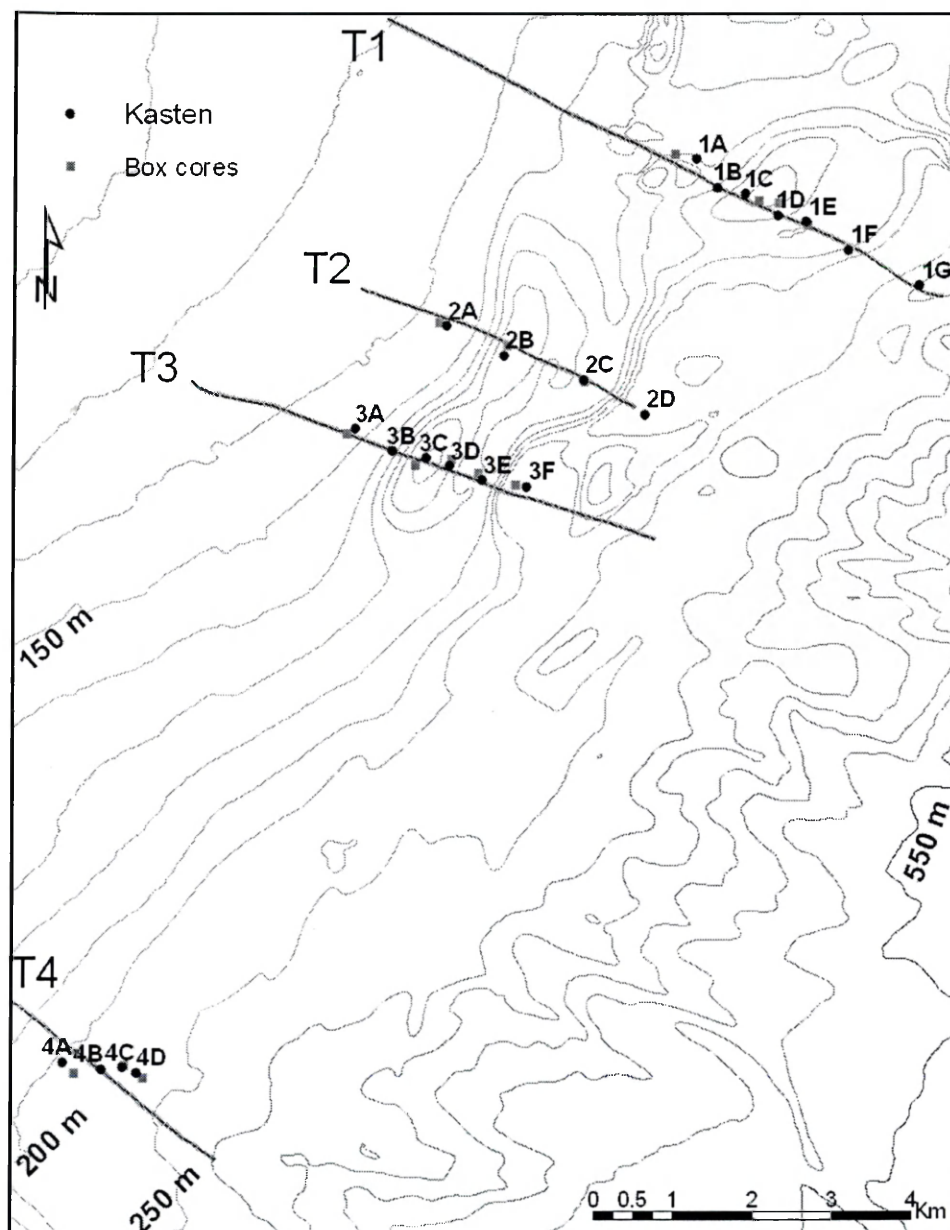


Fig 2: Enlarged section of Fig. 1 showing chirp lines, with transect numbers, and core names, which are consistent for box and kasten cores, and locations. The darker circles represent the kasten core locations grey squares represent the box cores.

Laboratory Techniques

The ^{210}Po procedure described in Nittrouer et al. (1979) for determining ^{210}Pb activity was used, with the only variation being that a ^{209}Po spike was used rather than the ^{208}Po spike. Through the assumption that ^{210}Pb and ^{210}Po are in secular equilibrium, the calculated ^{210}Po can be used as a proxy for the ^{210}Pb activity. Supported levels were estimated on an individual core basis by averaging values at depth where total ^{210}Pb activities became uniformly low. A common supported level could not be used due to the large variation in these values across the study region, ranging from .8 to 1.81 dpm g^{-1} . For ^7Be analysis gamma spectroscopy on planar intrinsic germanium detectors was used. Counts per minute (cpm) were converted to decays per minute (dpm) by taking into account the intensity of 477 keV photon for ^7Be and the detector efficiency measured through a North American Scientific NIST traceable mixed gamma standard. The samples were then dried and weighed in order to calculate dpm/g.

Sieving was used to separate the sand fraction from the silt and clay of the samples. Silt and clay fractions of the samples were quantified using pipette analysis based on Stokes' law (Gee and Bauder, 1986). The grain size itself may also be an indication of the sediment transport processes.

Selected samples were run for carbon, nitrogen, and $\delta^{13}\text{C}$. Sample preparation included freezing the samples in the case of the surface samples, however kasten cores that were analyzed had been stored at room temperature for 6 weeks and then at a temperature of 5°C for 24 weeks before analysis. The samples were then dried,

ground, and acidified within muffled scintillation vials using 10% HCl. Samples were then dried and weighed into tin capsules that had been rinsed with methanol. These samples were processed in the UC Davis Stable Isotope Facility through a continuous flow Isotope Ratio Mass Spectrometer (IRMS).

RESULTS

Shelf-edge Morphology

The shelf off the Waiapu River transforms from the gently sloping and smooth mid-shelf into an outer-shelf comprised of multiple depressions before reaching the slope that is dissected by canyons (Fig. 3). The southern region of the outer shelf can be described as a relatively smooth trough-like feature, within which a series of subtle shore parallel ridges are detected. Contrastingly, towards the northern section, 25 km directly off the mouth of the Waiapu, there exist small-scale localized basins including a set of bi-lobed basins, found along transects 2 and 3, as well as a single lobed basin slightly to the northeast along transect 1. These basins contain a steeply grading seafloor on the shoreward edge with a more gradual incline towards the topographic plateau.

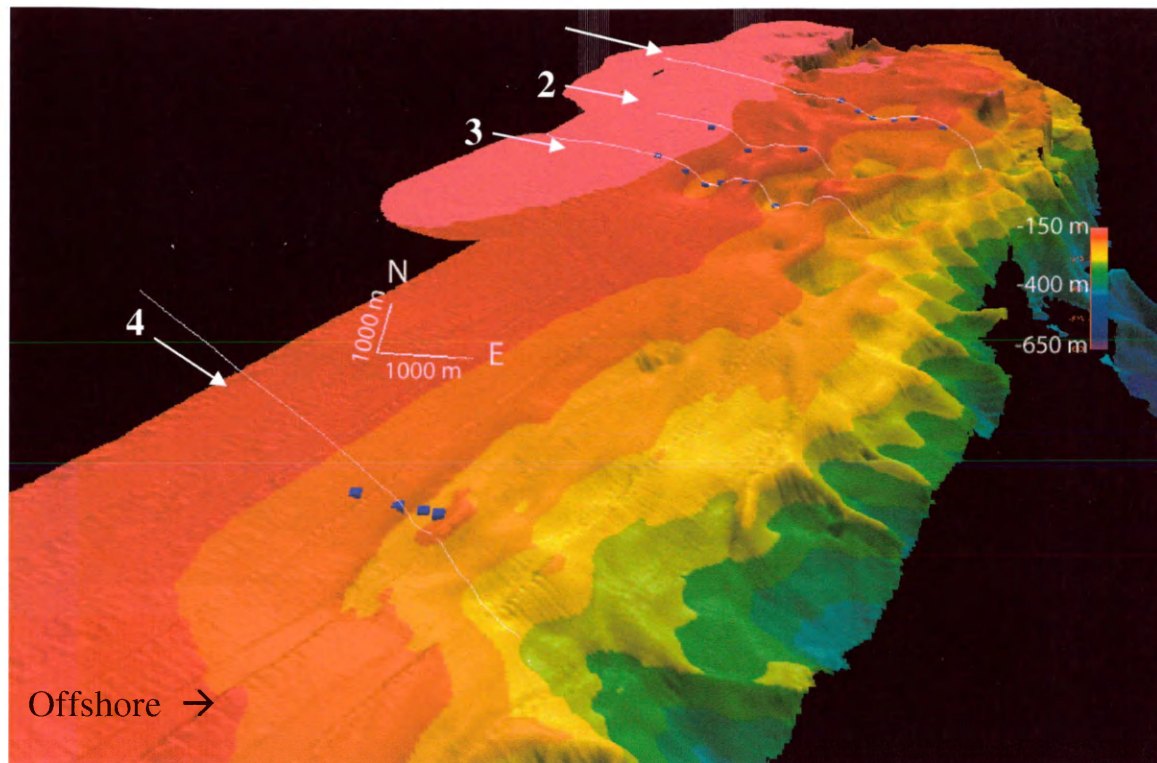


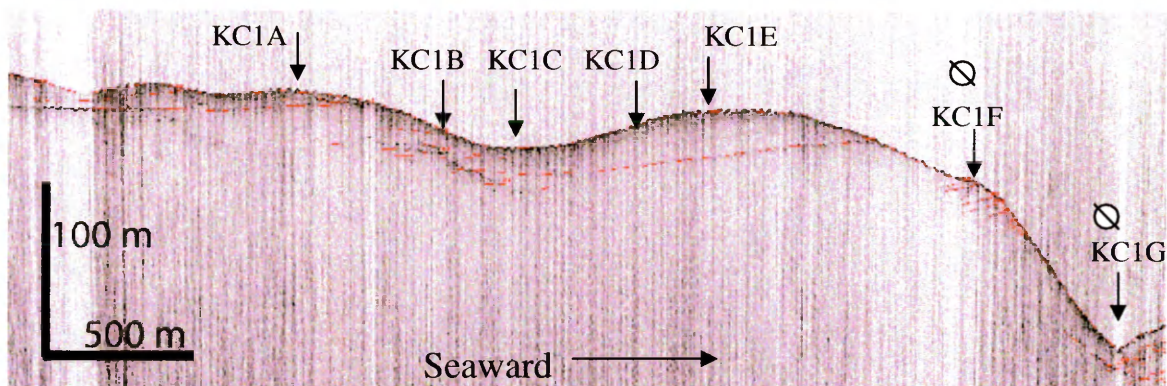
Fig. 3 Bathymetry of the shelf-edge visualized in 3D. Color scale bar on the right represents depth in meters. Black areas are locations where no data has been collected, numbers refer to the transect numbers, white lines represent chirp transects, and blue points indicate core locations.

Sub-bottom features

Chirp sub-bottom profiles were collected along the four across-shelf transects shown in Fig. 3. Approximate kasten core locations are represented by the black arrows within each figure (Figs. 4-7). Prominent reflectors have been outlined and are represented as red lines within the profiles. The circle with the slash indicates sites where no core was retrieved.

Transect 1: The chirp record for the northernmost transect is characterized by 2 deep reflectors (Fig. 4A). Swath and Chirp records reveal an apparent complexity shoreward of the basin, with a very steeply sloping region and multiple depressions shoreward of the sampling area. The most shoreward reflector is relatively flat and crops out at the shoreward edge of the basin. The seafloor alternates in this region, shoreward of the basin, between a series of bulged features beneath which exist shallower reflectors. These reflectors are deepest within the topographic highs and crop out on the seaward side of these relatively high regions. The other deep reflector appears within the main basin, near KC1C, which thickens moving towards the seaward plateau before cropping out where the gradient of the seafloor begins to steepen. Seaward of this are a series of truncated beds followed by a topographic low containing a number of weaker reflectors. Within this transect there is a general trend of increasing thickness above the most surficial reflector moving from the shelf towards the topographic high. This indicates that over the long-term it is likely that the topographic rise and high have been the zones of maximum deposition.

A)



B)

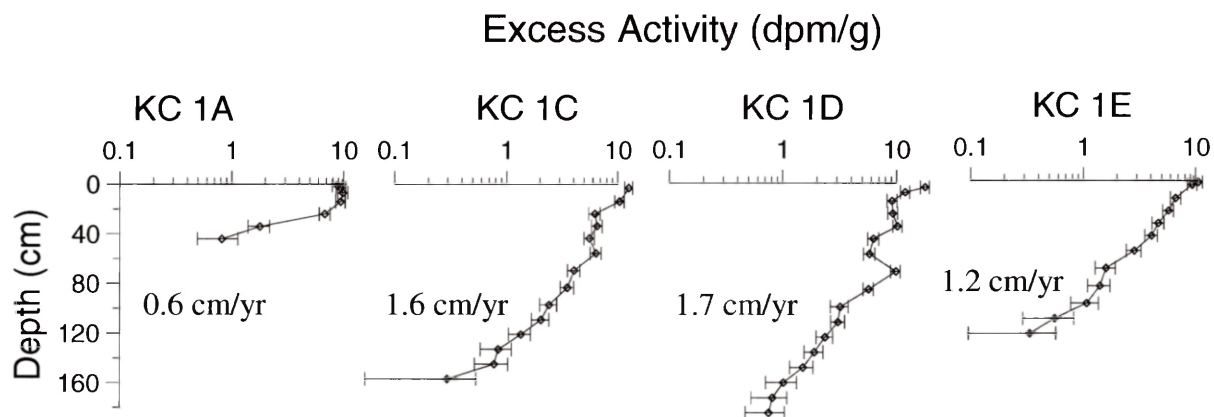


Fig. 4 A) Sub-bottom profile of the northern-most transect. Reflectors have been outlined in red. The main basin indicated by KC1C, the third arrow from the left. The circle with the slash indicates sites where no core was retrieved. B) ^{210}Pb profiles along transect 1, plotting excess activity versus depth. 3 of the 7 cores were left out because only short-cores were collected in these locations. The numbers found within each profile represent the accumulation rates.

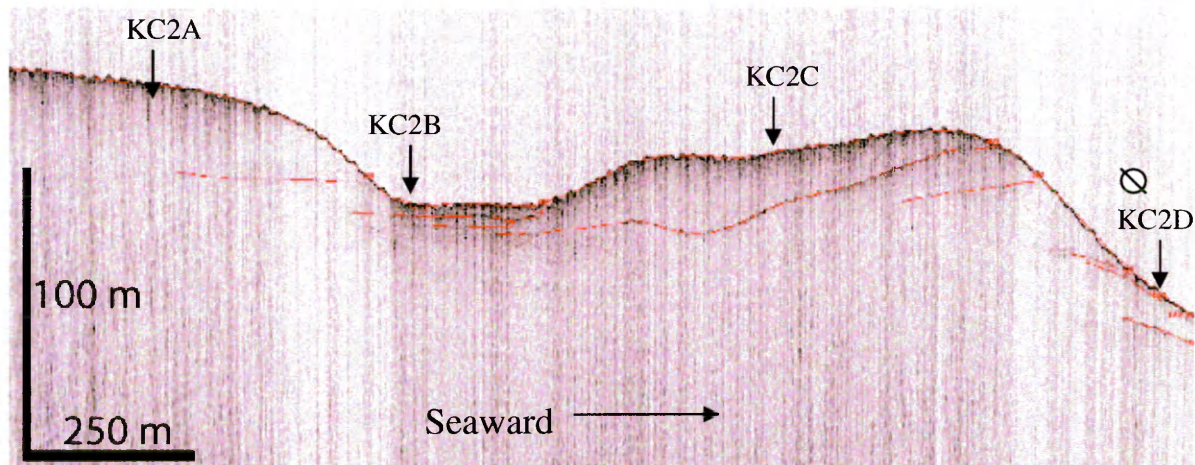
Transect 2:

This transect covers a much smaller area of the outer-shelf compared to the other three transects, only extending through one set of topographic lows and highs (Fig. 5A). The profile consists of a thick unit along the shelf just shoreward of the basin-low, the base of which outcrops along shoreward edge of the topographic low.

Within this basin there exists what appears to be a series of fill layers, represented by a number of strong reflectors. One of the deeper reflectors within the topographic low proceeds seaward, thinning and outcropping towards the topographic high.

Seaward, a number of truncated reflectors are observed, many of which appear where the seafloor begins to level.

A)



B)

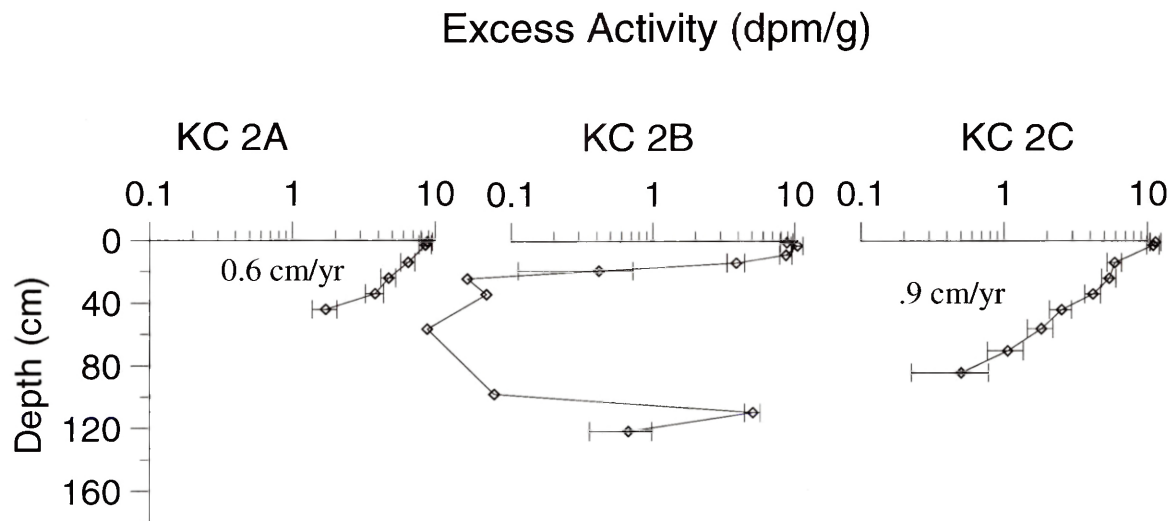
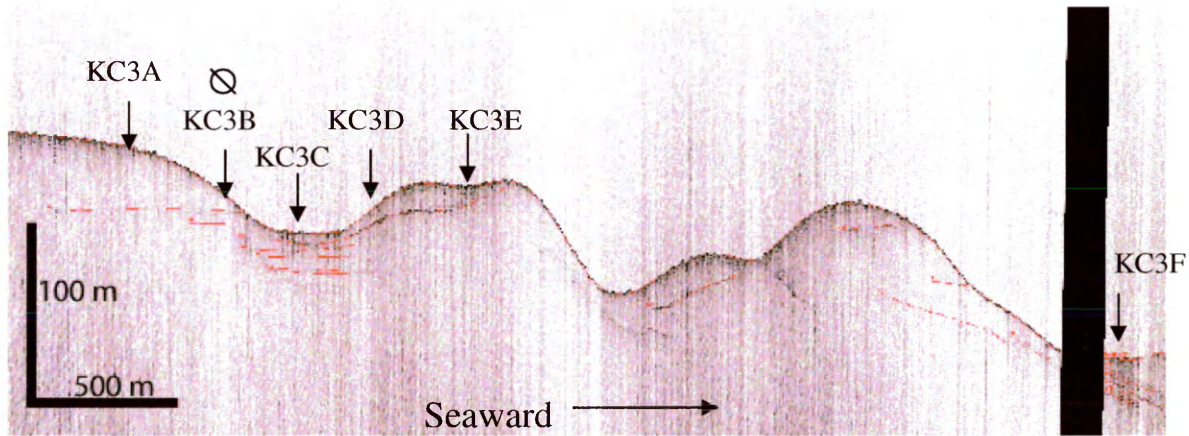


Fig. 5: A) Sub-bottom profile of transect 2, the northern lobe of the central basin, located to the south of transect 1. Basin indicated by KC2B. The circle with the slash indicates sites where no core was retrieved. B) Coinciding ^{210}Pb profiles with the exception of the core within the seaward depression. Values less than 0.1 dpm/s are at supported activity levels within calculated errors. Accumulation rates are included in cm/yr with the exception of KC2B, where supported levels could not be determined.

Transect 3: The profile passes through the southern portion of the central bi-lobed basin and presents areas of different depositional environments, shown by the varying thickness of the sub-bottom units as well as the numerous reflectors present across this portion of the shelf (Fig. 6A). The shelf shoreward of the basin is characterized by one deep reflector, ~50 meters deep, which thins and crops out along the shoreward edge of the basin. Within the basin-low there exist multiple reflectors indicating layers of fill with varying densities, including one that proceeds seaward towards the topographic rise and high, where the unit thickens and eventually crops out seaward of the basin. The drape along the seaward edge of the basin and plateau although thinner within this profile corresponds to that within transect 2. A similar drape is seen seaward of the second topographic low. Further seaward a third sharp incline exists in which a number of reflectors appear and proceed seaward towards the topographic low.

A)



B)

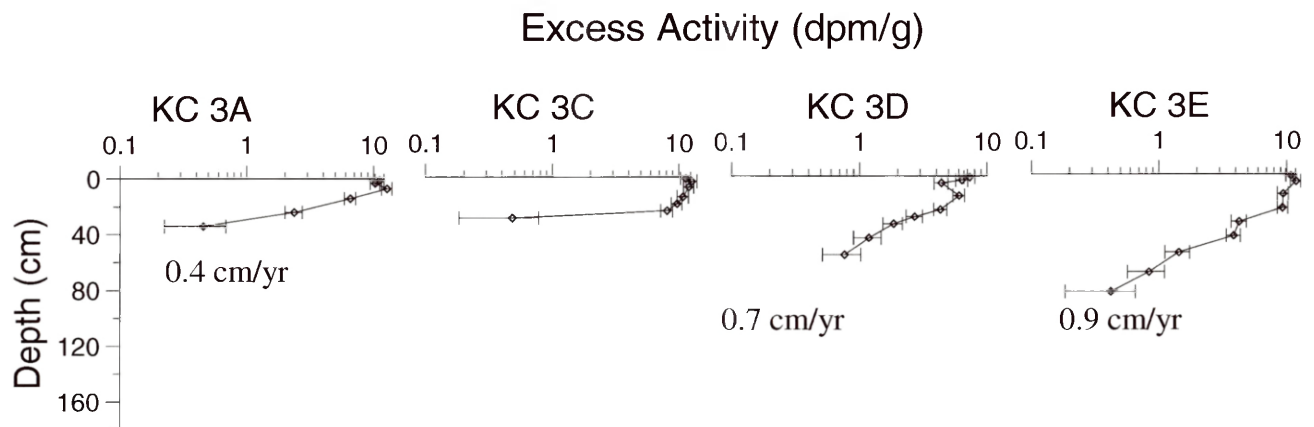
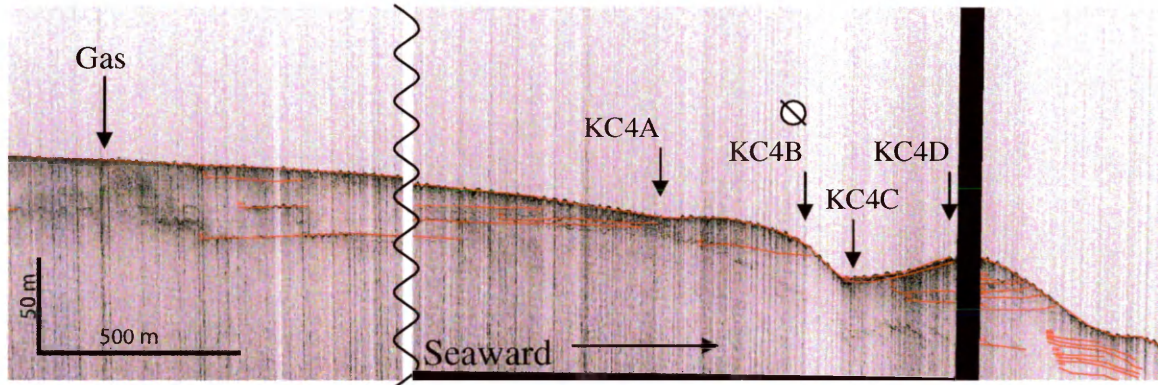


Fig. 6 A) Chirp record of transect 3 with topographic-low indicated by KC3C. No core was collected along the shoreward edge due to compacted sediment. The circle with the slash indicates sites where no core was retrieved. B) ^{210}Pb profiles for each kasten core excluding those where only short cores were collected. An accumulation rate was not calculated for KC3C because of the homogeneously mixed surface layer, which quickly reaches supported values.

Transect 4: Within the southernmost transect the profile contains a number of shallow reflectors along the shelf just shoreward of the topographic-low (Fig. 7A). With the exception of the deepest reflector all of these appear to crop out just seaward of the most shoreward core, KC4A. A widespread black area was seen within the upper 10 meters of the profile further inshore, which suggests that gas is present within the sediment. One reflector reappears on the shoreward edge of the depression and truncates directly past the topographic high, representing that along these features there appears to be a depositional region, with a thick drape-like layer, with the surrounding slopes acting as erosional features. From the locations of the cores, it can be seen that sampling occurred within two different stratigraphic units and within these specific units that there are varying thicknesses of material overlying the most recent reflector.

A)



B)

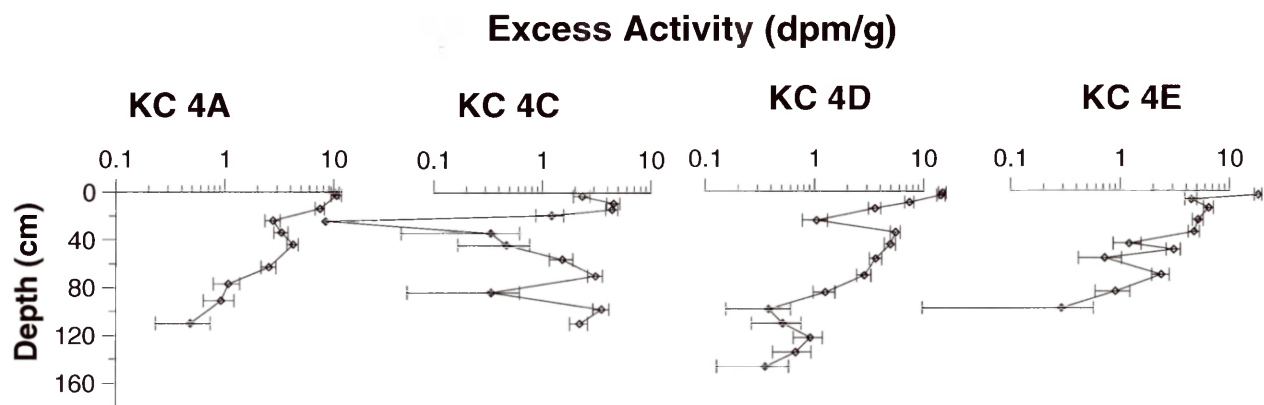


Fig. 7 A) Chirp sub-bottom profile along transect 4, running from in-shore to off-shelf going from the left to the right. The wavy line marks the location where a section of the transect has been removed in order to show the gas present further inshore in addition to the plateaued features. The black box shows an area that is missing data. The circle with the slash indicates sites where no core was retrieved. B) ^{210}Pb profiles along the same transect. The far right profile is from a core taken within a canyon incising the slope. No accumulation rates were calculated for these cores because these represent non-steady state profiles, allowing for no accumulation model to be fit to this data.

Pb-210

²¹⁰Pb accumulation rates were calculated only for the cores that displayed logarithmic decrease with depth because this is an indication of steady-state conditions. Using the constant flux, constant supply model, ²¹⁰Pb accumulation rates were calculated using the slope of the ²¹⁰Pb excess values within the non-supported region (e.g., Appleby and Oldfield, 1978).

Transect 1: The northernmost cores were collected along transect 1 (Fig. 4B). The ²¹⁰Pb profiles along transect 1 can be characterized as steady-state, allowing for the calculation of accumulation rates within all of the cores. Along this transect the highest rates of accumulation were within the topographic-low and on the seaward edge of the basin, with lowest rates found shoreward of the basin. The values along this transect represent the highest rates calculated across the entire outer-shelf.

Transect 2: Within transect 2 a total of 3 cores were collected, with a failed attempt at coring a seaward depression due to the presence of consolidated sediment in this region (Fig. 5B). One non-steady state profile exists in this transect located within the basin-low, KC2B. KC2B reaches supported levels of ²¹⁰Pb activity at a depth of around 25 cm and remains at these levels to a depth of 110 cm, where a spike in activity almost equal to surface activities is detected. The seaward edge of the basin contains the highest accumulation rates along this transect with a value of .9 cm yr⁻¹.

Transect 3: The cores within transect 3 are predominantly steady-state (Fig. 6B). There is a trend of increasing accumulation rates moving further offshore along this transect, with the exception of the topographic low. The profile for KC3C contains almost constant excess activity values within the top 25 cm, which quickly drop to supported values, although no down-core high activity spikes appear similar to that

within KC2B. These patterns of increasing accumulation rates moving offshore as well as the topographic-low correspond with observations detected within transect 2.

Transect 4: The southern transect is more of a ridged feature than a basin, but it can be seen from the chirp profile (Fig. 7A) that it could play the same type of role in sediment trapping due to the presence of a topographic high seaward of a depression. Within each of the ^{210}Pb profiles there exist low-activity spikes with higher values further downcore (Fig. 7B). These low-spikes are indicative of non-steady state accumulation within this region and are most significant within the last three cores, 4C, 4D, and 4E. KC4E was collected furthest seaward within a canyon that incises the slope. Because of the non-steady nature of these profiles, it was not possible to calculate accumulation rates for these cores. KC4C contains relatively low-activities throughout the core compared to values across the region, with maximum excess values of 4.5 dpm g^{-1} compared to average surface excess values of 14.5 dpm g^{-1} for this transect.

X-radiograph images

X-ray images were taken for each kasten core to assess the relative degree of physical versus biological sedimentary structure. Each transect varies in the extent of reworking, but some general trends are observed. One core has been selected for each transect with the exception of transect 2, where x-rays were incorrectly developed (Fig. 8). Within these cores transect 4 shows that physical processes dominate, with very little alteration of sediment by biological reworking. Within transect 3, the main source of mixing is biological, with little evidence of event

preservation. Transect 1 appears to exhibit characteristics from both transect 3 and 4, with evidence of some preservation of layers as well as biological reworking.

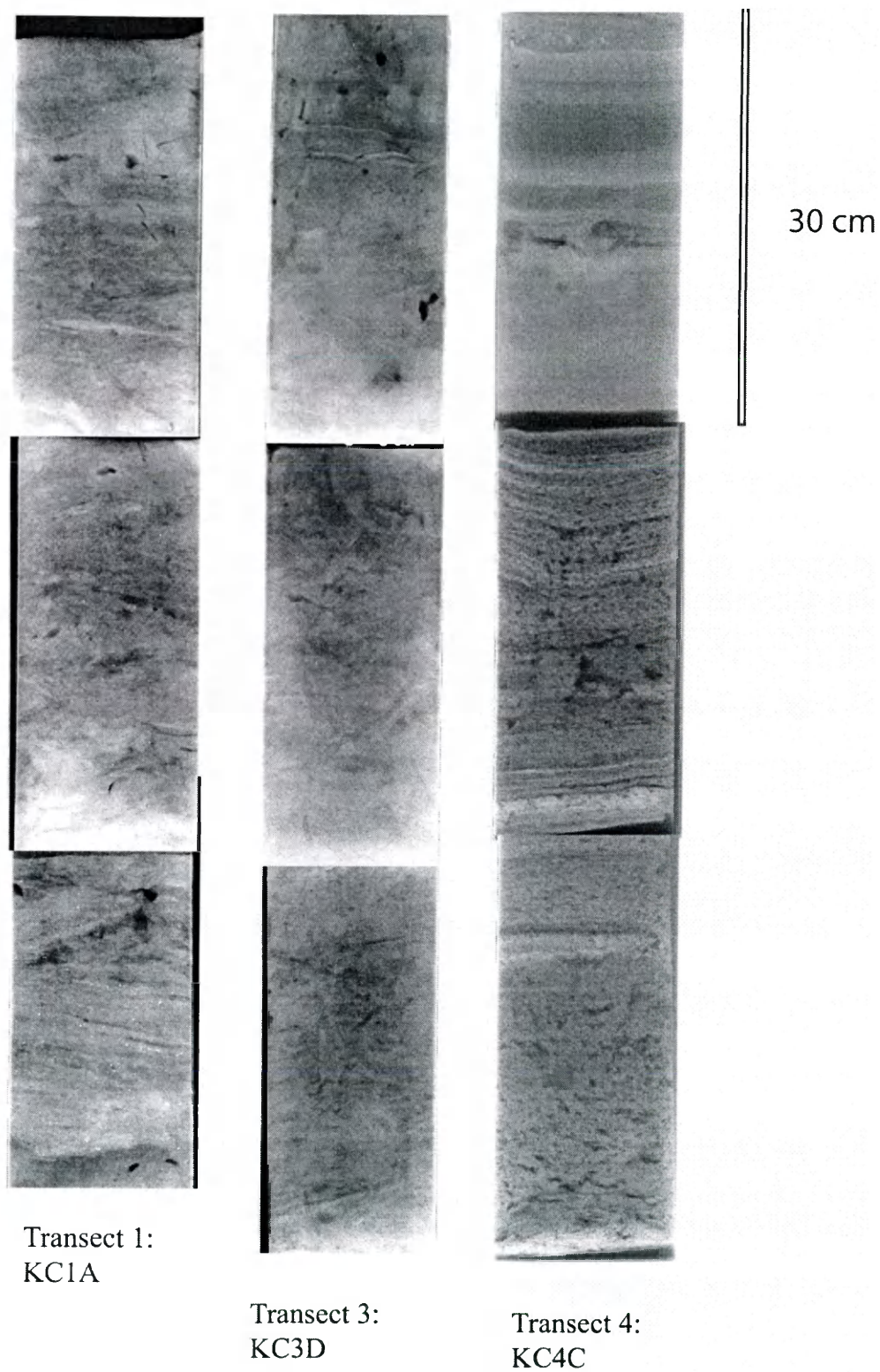


Fig. 8: X-ray images from transects 1, 3, and 4. Transect 2 was left out because poor x-rays were produced. The top images represent the surface of the core. Each square has a length of 30 cm with the exception of the third square in KC1A, which is only 25 cm long.

Grain Size

Calculations to normalize ^{210}Pb activity with respect to grain-size were made within a number of cores. This was done within both the ^{210}Pb excess window to determine whether low spikes in the data were in response to changes in grain-size as well as within the supported region to verify if the deviation in supported values across the region could be accounted for by grain-size (Table 1). Additionally grain-size analysis was performed for all of KC4C (Fig. 9). The trends that emerge from the grain-size data include the existence of predominantly clay-sized particles within the low ^{210}Pb activity spikes, whereas at the higher ^{210}Pb activities the largest percent of the sand fraction is found at ~8%. The ^{210}Pb total activities were corrected for grain-size because of the extreme variability of the profile (Fig. 10). Although there is a shift to higher ^{210}Pb activity when normalizing to 100% clay, the spikes remain. It can be seen that original supported values of the cores varied from .7 dpm g⁻¹ to 2.0 dpm g⁻¹ with three values falling outside of one standard deviation. When normalizing to 100% clay, supported values vary from 2.6 dpm g⁻¹ to 5.2 dpm g⁻¹ with two values falling outside of one standard deviation from the mean. A large variation in percent sand was observed, which is unexpected on the outer-shelf where the grain-size should predominantly consist of clay and silt sized particles.

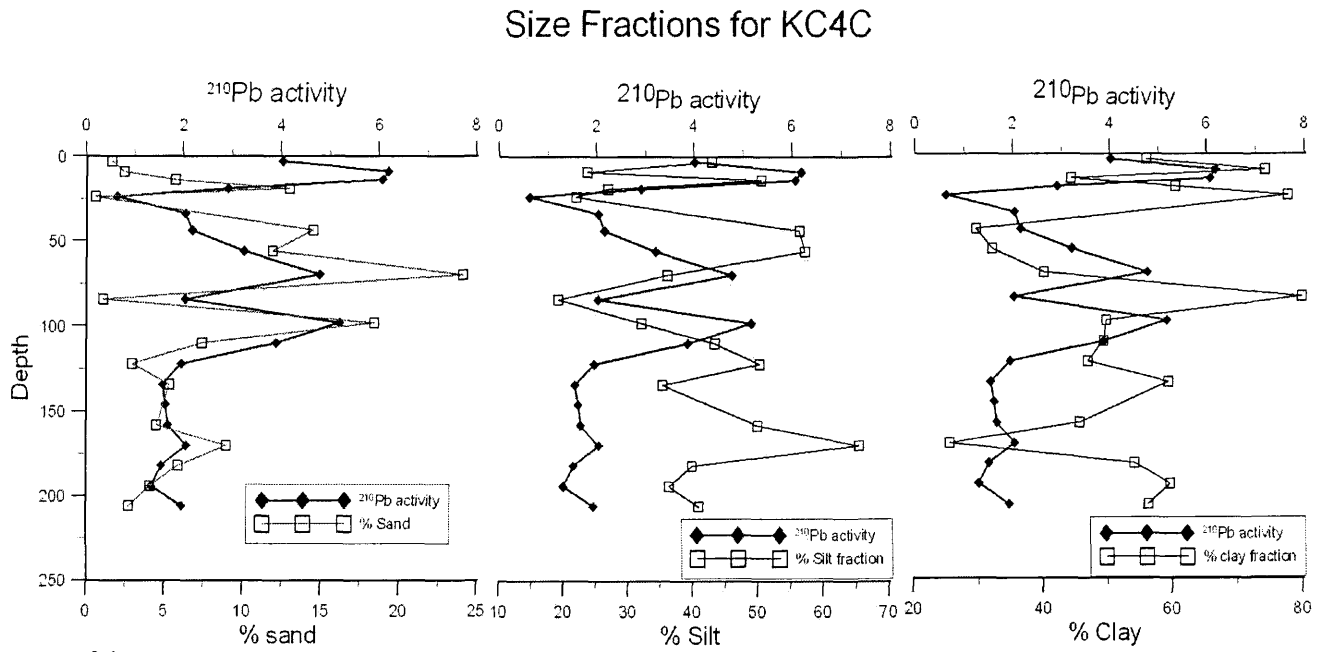


Fig. 9 ^{210}Pb activity for KC4C plotted with the sand, silt, and clay fractions.

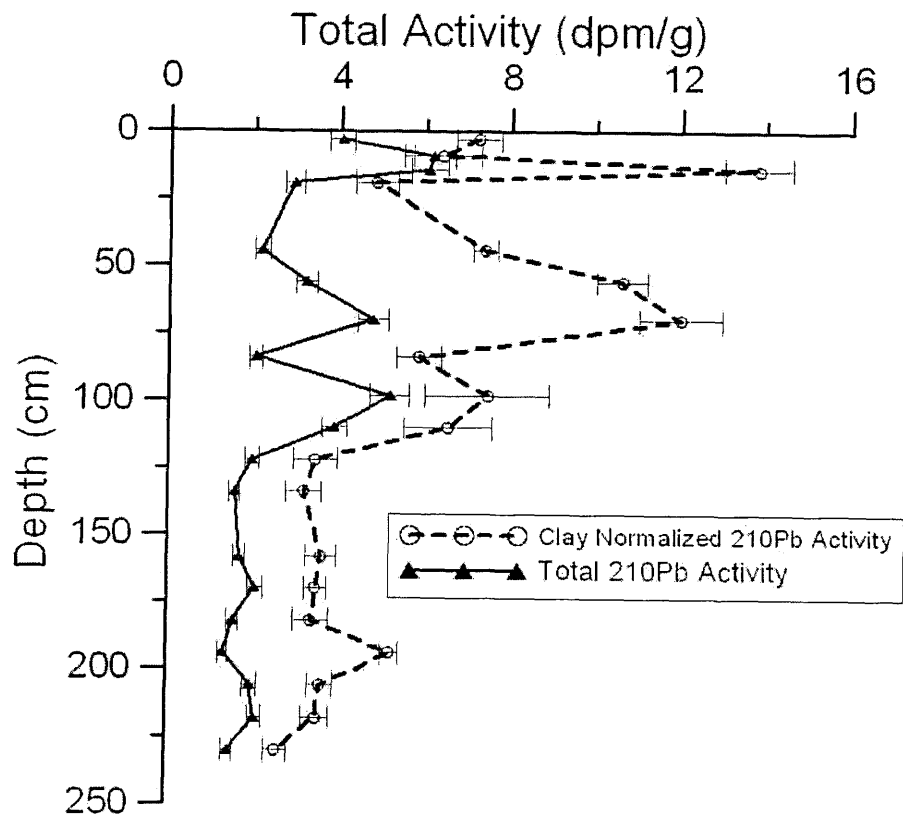


Fig. 10 Activity normalization has been performed for all of KC4C with the solid black line representing the total ^{210}Pb activity and the dotted line showing the total activity after it has been normalized to 100% clay.

Transect	Depth (cm) in the core	%clay	%silt	%sand	Supported	Normalized
					Total ^{210}Pb (dpm/s)	Total ^{210}Pb / %clay
KC2B	97-99	60.7	39.2	0.1	1.9	3.1
KC3A	69-71	22.7	48.6	28.7	0.9	4.0
KC3A	83-85	19.3	45.9	34.9	0.8	4.4
KC3A	97-99	21.0	49.8	29.2	0.8	3.7
KC3C	69-71	65.8	34.4	0.0	1.8	2.8
KC3C	83-85	63.1	36.9	0.0	2.0	3.1
KC3C	97-99	62.8	37.3	0.0	1.9	3.0
KC3D	83-85	19.0	42.0	39.0	1.0	5.2
KC3D	97-99	19.9	42.0	38.1	0.7	3.6
KC3F	109-111	64.2	35.8	0.0	1.8	2.8
KC3F	83-85	59.1	40.9	0.1	1.7	2.9
KC3F	97-99	60.7	39.2	0.0	1.8	3.0
KC4A	133-135	28.5	54.0	17.5	0.8	2.9
KC4A	145-147	30.6	50.2	19.2	0.9	2.9
KC4A	157-159	36.9	53.6	9.5	1.0	2.6
				Average=	1.3	3.3
				Std. Dev.=	0.5	0.7

Table 1 Grain size calculations for samples within the ^{210}Pb supported region, showing % of each size fraction, total ^{210}Pb activity, and 100% clay normalized activity. Samples from transects 2-4 have been run, with the majority coming from transect 3. The average and standard deviation for the total and normalized total are listed.

⁷Be distribution

The 0-1 cm interval was analyzed for all box core samples for ⁷Be activity (Table 2). Very low values were calculated across the outer shelf with many locations having no indication of a ⁷Be signal and others when accounting for error having no significant peak. Compared to values determined across the shelf, the outer shelf values represent only trace amounts of ⁷Be.

Core	Interval (cm)	A_0 (dpm/g)	A_0 error (dpm/g)
BC1A	0-1	0.00	0.00
BC1C	0-1	0.57	0.16
BC1C	1-2	0.08	0.05
BC1D	0-1	0.00	0.00
BC1E	0-1	0.18	0.11
BC1E	1-2	0.21	0.09
BC1E	2-3	0.12	0.05
BC1E	3-4	0.21	0.12
BC2A	0-1	0.00	0.00
BC2B	0-1	0.00	0.00
BC2C	0-1	0.17	0.11
BC2C	1-2	0.13	0.08
BC3A	0-1	0.00	0.00
BC3C	0-1	0.58	0.17
BC3C	1-2	0.15	0.09
BC3D	0-1	0.15	0.07
BC3E	0-1	0.00	0.00
BC3F	0-1	0.00	0.00
BC4A	0-1	0.11	0.06
BC4A	1-2	0.08	0.07
BC4A	2-3	0.15	0.09
BC4C	0-1	0.00	0.00
BC4D	1-2	0.00	0.00

Table 2: Box core locations, corresponding to kasten core names. The interval indicates the location in the core where the sample was collected. A_0 represents the ^7Be activity at time of sample collection and A_0 error represents the maximum associated error.

Carbon

$\delta^{13}\text{C}$, $\%C$, and $\%N$ were calculated for the box cores and 2 kasten cores, one within the southern region, KC4C, and one within the southern lobe of the central bilobed basin, KC3D. A predominantly terrestrial signature for KC4C was detected with more negative $\delta^{13}\text{C}$ values and low N/C values, represented by the atomic N/C ratio versus $\delta^{13}\text{C}$ values (Fig 10). KC3D with a predominantly steady-state profile shows a much more marine signature, with less negative $\delta^{13}\text{C}$ values compared to higher N/C values, with few intervals lying within the terrestrial region. The values for surface carbon are plotted as open diamonds and circles with shapes corresponding to the same transect as the carbon data for the kasten cores (Fig. 11). All of the surface carbon samples have a more marine influence compared to KC4C, but compare well with the down-core carbon of KC3D. Data was also collected for the box cores along transects 1 and 2, which are not shown, but whose values fall within the same region as these surface values.

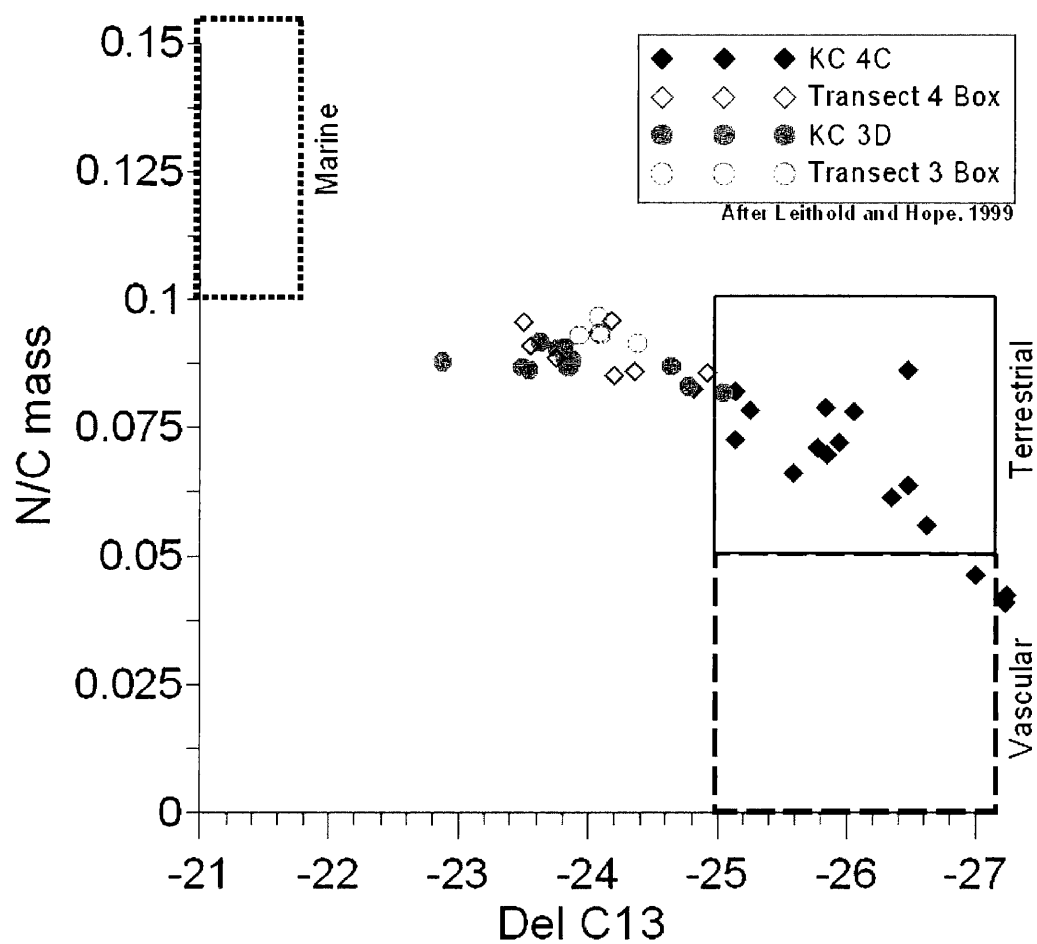


Fig. 11 Carbon data from 2 kasten cores, from transect 3 and 4, and all box cores located along these specific transects. Graph designed after Leithold and Hope (1999). Used to compare marine versus terrestrial signals at the surface as well as down-core.

DISCUSSION

Stratigraphic Interpretation

Northern Basins

Moving from the most northern transect towards the south some sub-bottom distinctions can be made (Figs. 4-7A). Along transect 1 shoreward of the basin the profile contains surface reflectors that are absent within transects 2 and 3. These additional reflectors may either be an influence of the very complex bathymetry just shoreward of the northern-most area, an indication that the northern-most basin is affected by different mechanisms compared to the bi-lobed basin, or a suggestion that the northern region may be a more active zone of deposition. Stratigraphically it appears that the shelf just shoreward of the basin is likely an area of lower deposition increasing towards the seaward plateau. The basin-low in transect 1 differs from those in transects 2 and 3 in the lack of reflectors present, but instead exclusively contains one deep reflector that crops out just seaward of the basin. This indicates that rather than the thin layers that were deposited within the central basin, sedimentation has remained fairly constant both temporally and spatially within this specific region.

The central two transects, 2 and 3, within the bi-lobed basin contain a main reflector present across the shelf as well as a shallower reflector which appears as a thin drape within the topographic low, thickening towards the seaward plateau. Within the topographic low, there are a series of strong reflectors, representing fill

within this area. The fill layers indicate deposition of layers with different densities, possibly showing that the source of material to these locations has varied over time. Alternatively, these density differences could be a result of de-watering of sediments or diagenesis. These reflectors within the basin-lows particularly the most seaward topographic-low in transect 2 may potentially be explained by the occurrence of gravity slumps of thick, older material from the slope just shoreward of these basins. Short cores were collected along all of these slopes, further indication that the slopes can be characterized as older more consolidated units. The thickness of the stratigraphic unit along the seaward edge of the basin decreases moving from transect 2 to transect 3, showing that there is a potential decrease in either sedimentation or preservation moving towards the south.

Southern shelf

The southern transect 4 (Fig. 7A) has evidence of methane gas within the sediment, which is commonly detected in organic rich sediment. This feature was seen exclusively within this profile. Multiple surface reflectors are also detected along the outer-shelf in this transect. One main reflector can be seen within the topographic low, which then crops out at the seaward plateau. The thickness of this reflector is fairly constant, indicating that deposition and subsequent preservation of material is occurring at the same rates along the topographic low and plateau. Along the steep gradient surfaces both shoreward and seaward of the topographic low and plateau, truncating reflectors are present, indicating that these are likely erosional features. An attempt at coring the shoreward edge was made, however the compacted

sediment did not allow for a core to be taken, which is further evidence towards the idea of this area acting as an erosive surface.

Recent Accumulation

^{137}Cs is a radioisotope commonly used in sediment geochronology to corroborate accumulation rates calculated through ^{210}Pb analysis. This method was not possible in the study site because of the very low concentrations of ^{137}Cs in the sediments. ^{137}Cs is an artificial radioisotope introduced into the atmosphere during nuclear reactor accidents and through nuclear weapons testing. The majority of nuclear testing occurred within the northern hemisphere and due to atmospheric circulation patterns, decreased amounts of this radioisotope were deposited within the southern hemisphere (Tsumune et al., 2003). This is an important factor to take into account when considering the ^{210}Pb data because without independent verification, the accumulation rates derived from ^{210}Pb represent maximum values (Benninger et al., 1979).

Northern Basins

Along all three northern transects the ^{210}Pb accumulation rates are lower along the shelf shoreward of the basins when compared to the side of the basin and plateau seaward of the basin-low (Figs. 4-6B). In both transect 2 and 3 the profiles within the topographic lows contain a surface layer with uniform ^{210}Pb activity, which quickly reaches supported levels. These ^{210}Pb profiles are likely showing a relatively uniform layer of sediment that has been mixed by either biological or physical processes overlaying an old erosive unit. The northern transect 1 differs from the other

transects in the high accumulation rates calculated for this area. Within the topographic low of transect 1 rates remain relatively high with a value of 1.6 cm yr^{-1} .

A significant variation in grain-size constituents was present within individual basins, specifically along transect 3. Within this transect the percent sand varied from 35% shoreward of the basin to 0% within the basin-low, back up to 39% along the seaward basin edge, then down to 0.1% in the most seaward depression. The change in grain-sizes along such a small region, with high sand fractions in the high accumulation rate areas and a very low sand fraction within the low accumulation cores indicates that these intervals represent collection of periods with differing transport regimes in the supported sections of individual cores.

Southern Shelf

Within transect 4 although all ^{210}Pb profiles can be classified as non-steady state, the three most seaward cores contain the greatest number of low-activity spikes (Fig. 7B). The more non-steady state cores are located within the topographic low, seaward plateau, and a canyon along the slope. The gradient along the shelf shoreward of the topographic low may not allow for the preservation of these low-spikes to the same extent as the other three sites. The existence of low ^{210}Pb activities, but with deep penetration in a strongly laminated core indicates that this location has had more of an impact from terrestrial flooding likely because it acts as a local depression allowing for increased trapping of sediments and therefore an increased preservation of these event layers. The existence of these low spikes within the seaward canyon indicates that the events causing these low spikes have affected regions as far seaward as the slope.

Combined recent accumulation across the region

By comparing the three transects from the north to the southernmost transect certain differences were observed. The most apparent distinction was in the steady versus non-steady nature of specific cores. The overall description of the profiles within the individual transects indicated that the three northern transects were predominantly steady-state whereas all four ^{210}Pb profiles from the southern transect could be described as non-steady state. The other variation across the region was related to the accumulation rates. The highest rates were calculated along the most northern transect indicating that this area is receiving a greater amount of material compared to the remaining northern transects.

Kasten core inventories of excess ^{210}Pb were calculated across the northern basin region in order to determine the degree of changes in ^{210}Pb scavenging and deposition across the outer shelf. Determining how inventories correspond with accumulation rates allows us to verify whether the accumulation rates are the primary factor affecting the core inventories or whether other factors may be involved, such as the degree of mixing within the water column or an offshore influx of high ^{210}Pb activity waters. Within the northern region it appears that inventory and accumulation rates relate fairly well with each other with an R^2 of .82 (Fig. 12). This is an indication that across this region the accumulation rates largely determine the core inventories.

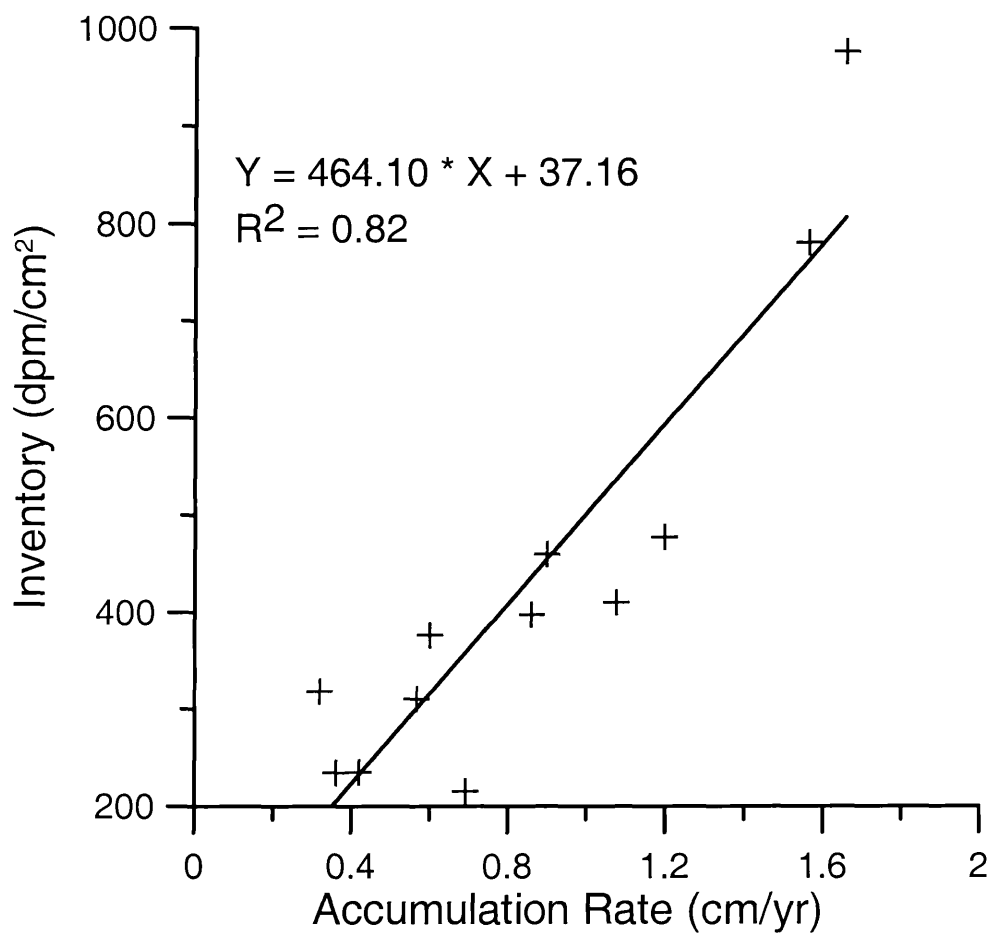


Fig. 12 Inventory vs. accumulation rate for all of the steady-state cores along transects 1-3. R^2 value indicates how well core inventories correlate to accumulation rates.

Carbon analysis was performed on surface samples (0-1 cm box core interval) across the entire study area. This data allows us to see what type of organic material was deposited within the few months preceding sample collection and therefore which areas of the shelf are presently receiving more of a terrestrial versus a more marine influence. The results indicate that the most recent sedimentation has a mixed marine and terrestrial signal. This indicates that across the study site the most surficial sediment has been delivered primarily by pelagic settling. ^7Be data supports this idea in the very low activities calculated across the region. The trace signal of ^7Be indicates that at the time of data collection there had been no recent flood events transporting and depositing large amounts of terrestrial material to the outer shelf.

Transport Mechanisms

Steady State

Steady-state profiles represent the logarithmic radioactive decay that accumulating sediments undergo. These profiles are expected when there is a constant supply of sediment with uniform activity values to a region. The northern basin area is dominated by these types of profiles with few exceptions.

The topographic-low in the northern transect contains a sub-bottom profile with no evidence of the various reflectors present in transects 2 and 3, which along with the high ^{210}Pb accumulation rates suggests that the northern basin has been a major depositional site in the past and continues to act as such at present. The preservation of laminations within this x-radiograph (Fig. 8) indicates that deposition is occurring at rates sufficiently rapid to advect sediment through the zone of mixing

before complete reworking can occur. The preserved layers also support the ^{210}Pb derived accumulation rates, eliminating the possibility that biological mixing has affected the decay profile. Carbon analysis of surface samples as well as one down-core, profile, KC3D, indicates that the material preserved within this region as well as that found at the sediment-water interface is primarily marine in nature.

The increasing accumulation rates moving south to north, decreasing degree of reworking shown within the x-radiographs, and the fairly uniform drape seen within the sub-bottom profile along the northern transect indicate that the dominant mechanism of transport to this region is through hypopycnal plume sedimentation, with little post-depositional alternation, whereas the bi-lobed basin is receiving a lower input of this hypopycnal sedimentation.

Non-steady state

A number of conditions allow for the development of non-steady state profiles. One possibility is that during extreme floods rates of ^{210}Pb removal from the water column are less efficient because the increased amount of sediments deplete available ^{210}Pb at greater rates than it is being supplied to the region through advection of oceanic waters (Sommerfield et al., 1999). Another prospective cause is that a slump of older material with low ^{210}Pb values was deposited into the system. Additionally, grain-size can have an effect on ^{210}Pb activity due to the change in scavenging potential of sediments depending on the surface area of the particles (He & Walling, 1995). Within larger particles, such as the sand fractions, smaller surface area to volume ratios exist compared to clay particles which have a very high surface area to volume ratio and therefore are capable of scavenging more ^{210}Pb compared to

the larger grains. Alternatively, gravity flows including hyperpycnal flows could be responsible for the intervals with decreased ^{210}Pb excess activities. When a density flow is produced it is transported along the seafloor with less interaction with the seawater compared to that of sediments delivered via surface plumes (Kineke et al., 2000).

Grain size analysis shows that the non-steady state profiles are not a function of varying grain-size throughout the length of the core. The persistence of the non-steady state profile after the ^{210}Pb activities had been normalized with respect to 100% clay indicates that grain-size was not the cause of the non-steady state nature of the cores (Fig. 10).

Carbon analysis was performed to determine the source of the organic material within the sediment and whether this could explain the intervals with decreased ^{210}Pb activities. One core from the southern region was chosen for carbon analysis. Results indicate that this non-steady state core has a strong terrestrial signature. This observation compared to the marine influence that was detected in the northern region show a divergence in the method of transport delivering sediment to the outer shelf.

Within the basin lows of the central bi-lobed basin, sub-bottom profiles filled with multiple reflectors and kasten cores that quickly reach supported ^{210}Pb values indicate that there is little modern sediment being deposited within this section. Evidence towards the idea of localized gravity slumping from steep slopes into topographic lows, first observed within the sub-bottom profiles, exists within the non-steady state ^{210}Pb profile of KC 2C, short cores obtained along the slopes (Fig. 4A,

5A, 6A, and 7A), and distinct layers of coarse grains from these regions. The x-radiograph for KC3F (Fig. 8), located within the most seaward topographic low contains one section of distinct layering, that when compared with the sub-bottom profile containing a series of reflectors cropping out at the surface of the slope indicates that gravity slumping is likely to have occurred.

“Event” flows

Surface carbon across the region indicates that primarily within the southern transect there is a discrepancy between the down-core data collected within KC4C and the surface sediment. Within the down-core profile the sediment has a dominantly terrestrial signal, however at the surface the signal is substantially more marine. This implies that the majority of material preserved in this region is a result of sedimentation during flood events and that the more marine dominated sediment although present at the surface is not preserved within the sediment record.

Grain-size analysis revealed that the layers with low ^{210}Pb activity correspond to a predominance of fine-grain clay sized particles at these intervals. This data is an indication that the sequences deposited during flood events consist of fine-grain material. This observation is consistent with data collected off of the Eel River after a 1997 flood event (Sommerfield et al., 1999).

The sub-bottom profile characterized by multiple reflectors and evidence of gas along the shelf suggests that over a much longer time-scale this area was also an active site of sediment deposition. The non-steady state profiles with low overall excess ^{210}Pb activity, terrestrial signal, and grain-size observations indicate that the likely explanation for the low-spikes of ^{210}Pb activity are due to density flows

transporting sediment to the south along transect 4 affecting not only the outershell within this region, but also seaward of the shelf-edge within a canyon along the slope. On the other hand, the northern area seems to be predominantly affected by pelagic settling from the buoyant surface plume. In contrast to the initial hypothesis that the northern basins would act as a trapping mechanism for hyperpycnal flows, these features appear to be primarily bypassed by present-day sediment having very low accumulation rates within the topographic lows, with a relatively uniform surface mixed layer, and slumping from the corresponding slopes acting as a potential input for sediment, with the exception of the most northern basin.

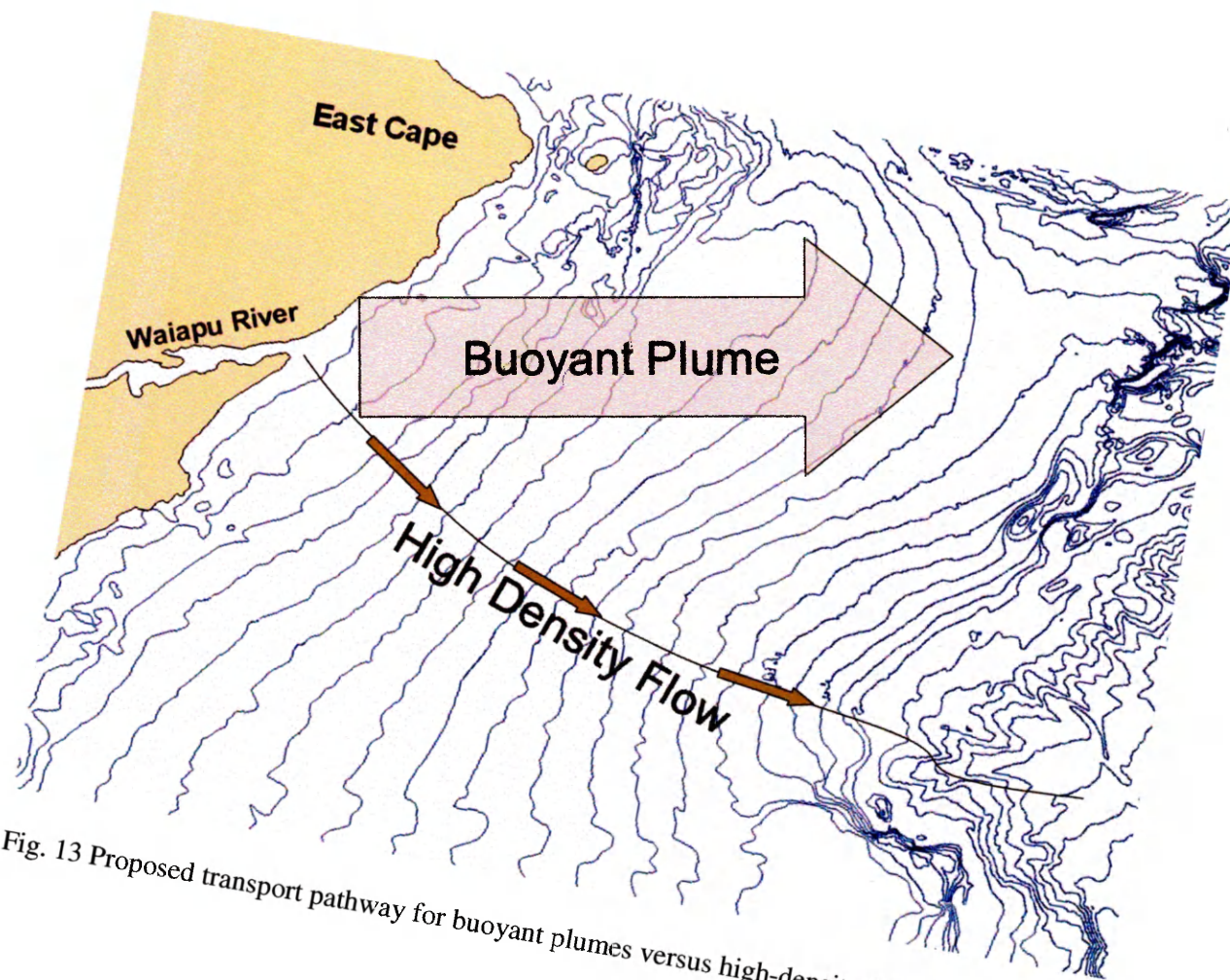


Fig. 13 Proposed transport pathway for buoyant plumes versus high-density flows.

CONCLUSIONS

Major conclusions for this study include:

- Initially it was hypothesized that buoyant transport, hyperpycnal flows, or some combination of these may be acting to transport sediment from the Waiapu mouth to the shelf-edge. Data suggests that both density flows and pelagic settling are likely transport mechanisms.
- The outer-shelf off the Waiapu River has distinct transport pathways for both high-density flows as well as for buoyant surface plumes. During high-density transport, sediment flows rapidly from the river mouth to the south proceeding offshore to the outer-shelf. During times of lower sediment concentration the plume will discharge from the river-mouth flowing slightly north and depositing sediment via pelagic settling.
- Sedimentation patterns not only vary from north to south across the shelf, but also within individual basins. A likely explanation for the variability of sediment accumulation within individual basins could be due to local physical processes, including slumping, shelf-edge currents, eddy formation, and channeling of flow through basin lows, which may act to resuspend and erode sediment within the basins.

- By looking at the ^{210}Pb profiles in addition to the chirp sub-bottom records it can be seen that the short-term 100-year accumulations compare well with the long-term patterns.
- Present-day morphology of this region has resulted from a combination of tectonic forces and local accumulation patterns.

APPENDIX A

Kasten and Box Core Locations

Kasten Cores						
Core name	Latitude (S)	Longitude (E)	Depth (m)	Length (cm)	Date of Collection	
1B	37 45.7433	178 46.9890	184	15	5/27/2004	
1C	37 45.7848	178 47.1760	200	226	5/27/2004	
1D	37 45.9804	178 47.3993	195	221	5/27/2004	
1D	37 45.9774	178 47.5947	181	192	5/27/2004	
1G	37 46.4118	178 48.3620	311	2	5/27/2004	
1F	37 46.1700	178 47.8739	191	1	5/27/2004	
4A	37 51.7370	178 42.5548	206	218	5/29/2004	
4B	37 51.7841	178 42.8137	216	2	5/29/2004	
4C	37 51.7722	178 42.9607	229	185	5/29/2004	
4D	37 51.8097	178 43.0571	225	232	5/29/2004	
3G	37 49.5375	178 50.1610	658	253	5/22/2004	
4E	37 54.5306	178 50.1191	747	208	5/30/2004	
2D	37 47.3041	178 46.5039	231	2	6/1/2004	
2C	37 47.0660	178 46.0847	164	151	6/1/2004	
2B	37 46.8985	178 45.5343	187	182	6/1/2004	
2A	37 46.6961	178 45.1507	143	96	6/1/2004	
1H	37 47.2540	178 50.8906	695	175	6/1/2004	
3A	37 47.4022	178 44.5330	148	114	5/24/2004	
3B	37 47.5531	178 44.7866	172	40	5/24/2004	
3C	37 47.6028	178 45.0113	201	199	5/24/2004	
3D	37 47.6567	178 45.1693	189	147	5/24/2004	
3E	37 47.7512	178 45.3916	177	187	5/24/2004	
3F	37 47.7964	178 45.6993	233	166	5/24/2004	
1A	37 45.5492	178 46.8420	169	85	5/27/2004	

Box Cores				
Core name	Latitude (S)	Longitude (E)	Depth (m)	Date of Collection
BC1E	37 46.0066	178 47.5968	183	5/27/2004
BC1D	37 45.8544	178 47.4004	199	5/27/2004
BC3G	37 49.4803	178 50.0449	656	5/22/2004
BC3A	37 47.4394	178 44.4678	148	5/30/2004
BC3C	37 47.6520	178 44.9341	199	5/30/2004

Core name	Latitude (S)	Longitude (E)	Depth (m)	Date of Collection
BC3D	37 47.6154	178 45.1813	188	5/30/2004
BC3E	37 47.7127	178 45.3655	178	5/30/2004
BC3F	37 47.7889	178 45.6174	232	5/30/2004
BC1A	37 45.5206	178 46.6928	171	5/30/2004
BC1C	37 45.8380	178 47.2658	202	5/30/2004
BC4A	37 51.8216	178 42.6288	205	5/30/2004
BC4C	37 51.7657	178 42.9640	228	5/30/2004
BC4D	37 51.8514	178 43.0949	218	5/30/2004
BC4E	37 54.5693	178 50.1309	747	5/30/2004
BC2A	37 46.6823	178 45.0958	142	6/1/2004
BC2B	37 46.8365	178 45.5560	186	6/1/2004
BC2C	37 47.0855	178 46.0838	163	6/1/2004
BC1H	37 47.2041	178 50.8267	695	6/1/2004

APPENDIX B

Definition of Terms and Equations used to determine excess ²¹⁰Pb Activity

²⁰⁹Po_{GA} = Gross Area of ²⁰⁹Po at time of counting

²¹⁰Po_{GA} = Gross Area of ²¹⁰Po at time of counting

S_{wt} = sample weight

A_s = Spike activity at time of calibration

V_s = Spike volume

²⁰⁹Po_{corr} = Decay correction term for ²⁰⁹Po from time of spike calibration to counting

²¹⁰Po_{corr} = Decay correction term for ²¹⁰Po from time of plating to counting

²¹⁰Pb_{corr} = Decay correction term for ²¹⁰Pb from time of sample collection to counting

A_{uncorr} = Uncorrected ²¹⁰Pb activity

A_{xs} = Excess ²¹⁰Pb activity

A_{supp} = Supported ²¹⁰Pb activity = mean activities for the section of the core where background levels have been reached

T_{spike} = date spike was calibrated

T_{coll} = Date of sample collection

T_{plt} = Date of plating

T_{cnt} = Date sample was counted

Er = error of A_{xs}

$${}^{209}\text{Po}_{\text{corr}} = \exp [(\ln(2)/102) * ((T_{\text{cnt}} - T_{\text{spike}}) / 365.25)] \quad (1\text{-B})$$

$${}^{210}\text{Po}_{\text{corr}} = \exp [(\ln(2)/(138.4/365.25)) * ((T_{\text{cnt}} - T_{\text{plt}}) / 365.25)] \quad (2\text{-B})$$

$${}^{210}\text{Pb}_{\text{corr}} = \exp [(\ln(2)/22.26) * ((T_{\text{cnt}} - T_{\text{coll}}) / 365.25)] \quad (3\text{-B})$$

$$A_{\text{uncorr}} = [(^{210}\text{POGA} / ^{209}\text{POGA}) * ((A_s * V_s * ^{209}\text{PO}_{\text{corr}}) / S_{\text{wt}})] / ^{210}\text{PO}_{\text{corr}} \quad (4\text{-B})$$

$$A_{\text{xs}} = (A_{\text{uncorr}} - A_{\text{supp}}) / ^{210}\text{Pb}_{\text{corr}} \quad (5\text{-B})$$

$$\text{Er} = ((((((((((((^{210}\text{POGA} / ^{210}\text{POGA}^2 + ^{209}\text{POGA} / ^{209}\text{POGA}^2)^{.05} * ^{210}\text{POGA} / ^{209}\text{POGA}) / (^{210}\text{POGA} / ^{209}\text{POGA})) + ((3 * V_s * ^{209}\text{PO}_{\text{corr}}) / (V_s * ^{209}\text{PO}_{\text{corr}}))) * ((^{210}\text{POGA} / ^{209}\text{POGA}) * (V_s * ^{209}\text{PO}_{\text{corr}}))) / ((^{210}\text{POGA} / ^{209}\text{POGA}) * V_s * ^{209}\text{PO}_{\text{corr}}) + (.01 / S_{\text{wt}})) * [((^{210}\text{POGA} / ^{209}\text{POGA}) * (V_s * ^{209}\text{PO}_{\text{corr}})) / S_{\text{wt}}] / ^{210}\text{PO}_{\text{corr}}) + .12) / ^{210}\text{Pb}_{\text{corr}}) \quad (6\text{-B})$$

APPENDIX C

²¹⁰Pb Depths and Activities

The equations listed in Appendix B were used to calculate ²¹⁰Pb activities.

***** indicates values that have been averaged to calculate the supported activity (A_{supp}) for that specific core. Refer to definitions in Appendix B for a description of the abbreviated column labels.

TRANSECT 1

Station	Midpoint	A_{uncorr} at T_{plt}	Absolute Error A_{uncorr} at T_{plt}	A_{xs} at T_{coll}	Absolute Error A_{xs} at T_{coll}	A_{uncorr} values used for A_{supp} calculation and A_{supp}
KC1A	1	10.12	0.77	8.84	0.91	
KC1A	3	10.79	0.81	9.49	0.94	
KC1A	7	11.17	0.86	9.91	1.00	
KC1A	14	10.75	0.80	9.45	0.93	
KC1A	24	8.19	0.60	6.85	0.73	
KC1A	34	3.24	0.26	1.83	0.39	
KC1A	44	2.28	0.20	0.86	0.32	
KC1A	56	1.56	0.15	0.13	0.27	*****1.56
KC1A	70	1.22	0.11	-0.21	0.23	*****1.22
KC1A	77	1.18	0.11	-0.25	0.23	*****1.18
KC1A	84	1.76	0.16	0.34	0.29	*****1.76
						$A_{\text{supp}} = 1.43$
KC1B	3	10.47	0.76	-----	-----	Short core, A_{supp}
KC1B	14	6.79	0.50	-----	-----	could not be
						calculated
KC1C	3	13.36	0.93	12.52	1.07	
KC1C	14	11.26	0.85	10.40	0.98	
KC1C	24	7.16	0.61	6.26	0.74	
KC1C	34	7.48	0.63	6.58	0.75	
KC1C	44	6.50	0.48	5.59	0.61	
KC1C	56	7.30	0.59	6.40	0.72	
KC1C	70	4.98	0.39	4.06	0.51	
KC1C	84	4.48	0.35	3.55	0.48	
KC1C	98	3.37	0.29	2.43	0.42	
KC1C	110	3.00	0.25	2.06	0.37	
KC1C	122	2.30	0.18	1.36	0.30	
KC1C	134	1.80	0.14	0.85	0.26	
KC1C	146	1.73	0.13	0.78	0.26	
KC1C	158	1.25	0.12	0.30	0.24	
KC1C	170	1.03	0.10	0.07	0.22	*****.99
KC1C	182	0.99	0.11	0.02	0.24	

Station	Midpoint	A_{uncorr} at T_{plt}	Absolute Error A_{uncorr} at T_{plt}	A_{xs} at T_{coll}	Absolute Error A_{xs} at T_{coll}	A_{uncorr} values used for A_{supp} calculation and A_{supp}
KC1C	194	1.00	0.08	0.04	0.21	*****1.00
KC1C	206	0.90	0.07	-0.06	0.20	*****.90
						$A_{\text{supp}} = .96$
KC1D	3	18.97	1.45	17.92	1.59	
KC1D	7	13.05	0.98	12.02	1.12	
KC1D	14	10.31	0.80	9.18	0.93	
KC1D	24	10.46	0.79	9.33	0.92	
KC1D	34	11.39	0.83	10.26	0.95	
KC1D	44	7.48	0.58	6.32	0.70	
KC1D	56	7.01	0.53	5.84	0.66	
KC1D	70	11.06	0.83	9.93	0.96	
KC1D	84	6.89	0.47	5.72	0.60	
KC1D	98	4.41	0.44	3.22	0.57	
KC1D	110	4.29	0.31	3.09	0.44	
KC1D	122	3.57	0.26	2.38	0.39	
KC1D	134	3.10	0.24	1.91	0.37	
KC1D	146	2.71	0.23	1.52	0.35	
KC1D	158	2.23	0.18	1.02	0.31	
KC1D	170	2.03	0.15	0.82	0.28	
KC1D	182	1.97	0.16	0.76	0.28	
KC1D	194	1.42	0.11	0.19	0.24	
KC1D	206	1.33	0.12	0.11	0.24	*****1.33
KC1D	218	1.23	0.10	0.00	0.23	*****1.23
						$A_{\text{supp}} = 1.28$
KC1E	1	11.47	0.81	10.57	0.95	
KC1E	3	10.34	0.75	9.36	0.88	
KC1E	14	7.69	0.59	6.68	0.72	
KC1E	24	6.77	0.50	5.76	0.63	
KC1E	34	5.69	0.43	4.67	0.55	
KC1E	44	5.10	0.41	4.07	0.53	
KC1E	56	3.91	0.30	2.86	0.42	
KC1E	70	2.67	0.20	1.61	0.33	
KC1E	84	2.48	0.20	1.42	0.32	
KC1E	98	2.14	0.17	1.08	0.29	
KC1E	110	1.63	0.15	0.56	0.27	
KC1E	122	1.41	0.12	0.34	0.24	
KC1E	134	1.11	0.10	0.04	0.22	*****1.11
KC1E	146	1.10	0.10	0.02	0.22	*****1.10
KC1E	158	1.06	0.10	-0.02	0.22	*****1.06
						$A_{\text{supp}} = 1.09$

Station	Midpoint	A_{uncorr} at T_{plt}	Absolute Error A_{uncorr} at T_{plt}	A_{xs} at T_{coll}	Absolute Error A_{xs} at T_{coll}	A_{uncorr} values used for A_{supp} calculation and A_{supp}
KC1F	No core retrieved		-----	-----	-----	
KC1G	No core retrieved		-----	-----	-----	
KC1H	1	26.12	1.82	25.43	1.97	
KC1H	3	21.98	1.69	21.16	1.83	
KC1H	14	6.37	0.60	5.34	0.73	
KC1H	24	3.02	0.23	1.94	0.36	
KC1H	34	2.57	0.22	1.49	0.34	
KC1H	44	1.73	0.15	0.63	0.27	
KC1H	56	1.24	0.11	0.14	0.23	
KC1H	70	1.21	0.11	0.11	0.23	
KC1H	84	1.09	0.11	-0.01	0.23	****1.09
KC1H	98	1.04	0.10	-0.06	0.22	****1.04
KC1H	110	1.17	0.12	0.07	0.24	****1.17
						$A_{\text{supp}} = 1.10$

TRANSECT 2

Station	Midpoint	A_{uncorr} at T_{plt}	Absolute Error A_{uncorr} at T_{plt}	A_{xs} at T_{coll}	Absolute Error A_{xs} at T_{coll}	A_{uncorr} values used for A_{supp} calculation and A_{supp}
KC2A	1	9.61	0.65	8.86	0.79	
KC2A	3	9.37	0.75	8.60	0.88	
KC2A	14	7.30	0.61	6.49	0.74	
KC2A	24	5.57	0.43	4.74	0.55	
KC2A	34	4.65	0.42	3.81	0.55	
KC2A	44	2.58	0.21	1.71	0.33	
KC2A	56	0.98	0.08	0.09	0.21	****.98
KC2A	70	0.89	0.09	-0.01	0.21	****.89
KC2A	84	0.81	0.08	-0.09	0.20	****.81
						$A_{\text{supp}} = .89$
KC2B	1	10.50	0.77	8.81	0.90	
KC2B	3	12.16	0.87	10.46	1.00	
KC2B	9	10.37	0.75	8.68	0.88	
KC2B	14	5.64	0.41	3.86	0.54	
KC2B	19	2.20	0.18	0.38	0.30	
KC2B	24	1.84	0.16	0.02	0.29	****1.84
KC2B	34	1.86	0.16	0.04	0.29	****1.86
KC2B	44	1.78	0.16	-0.05	0.28	****1.78

Station	Midpoint	A_{uncorr} at T_{plt}	Absolute Error A_{uncorr} at T_{plt}	A_{xs} at T_{coll}	Absolute Error A_{xs} at T_{coll}	A_{uncorr} values used for A_{supp} calculation and A_{supp}
KC2B	56	1.82	0.15	-0.01	0.28	*****1.82
KC2B	84	1.79	0.15	-0.04	0.27	*****1.79
KC2B	98	1.87	0.15	0.04	0.27	*****1.87
KC2B	110	6.81	0.50	5.04	0.63	
KC2B	110	6.77	0.51	5.06	0.64	
KC2B	122	2.45	0.18	0.64	0.31	

 $A_{supp} = 1.83$

KC2C	1	12.39	0.85	11.37	0.98	
KC2C	3	12.03	0.97	10.97	1.10	
KC2C	14	7.04	0.54	5.91	0.67	
KC2C	24	6.54	0.49	5.41	0.62	
KC2C	34	5.32	0.40	4.17	0.53	
KC2C	44	3.69	0.32	2.52	0.44	
KC2C	56	3.00	0.24	1.82	0.36	
KC2C	70	2.25	0.17	1.07	0.30	
KC2C	84	1.69	0.15	0.51	0.28	
KC2C	98	1.41	0.13	0.22	0.26	
KC2C	110	1.18	0.12	-0.01	0.25	*****1.18
KC2C	122	1.15	0.10	-0.05	0.22	*****1.15
KC2C	134	1.26	0.12	0.06	0.24	*****1.26

 $A_{supp} = 1.20$

TRANSECT 3

Station	Midpoint	A_{uncorr} at T_{plt}	Absolute Error A_{uncorr} at T_{plt}	A_{xs} at T_{coll}	Absolute Error A_{xs} at T_{coll}	A_{uncorr} values used for A_{supp} calculation and A_{supp}
KC3A	1	11.67	0.82	11.08	0.96	
KC3A	3	10.81	0.76	10.19	0.91	
KC3A	7	13.20	1.01	12.64	1.15	
KC3A	14	7.19	0.55	6.49	0.68	
KC3A	24	3.11	0.23	2.31	0.36	
KC3A	34	1.25	0.10	0.39	0.23	
KC3A	56	0.92	0.08	0.06	0.21	*****.92
KC3A	70	0.92	0.08	0.06	0.21	*****.92
KC3A	84	0.84	0.08	-0.02	0.20	*****.84
KC3A	98	0.77	0.07	-0.10	0.19	*****.77

 $A_{supp} = .86$

Station	Midpoint	A_{uncorr} at T_{plt}	Absolute Error A_{uncorr} at T_{plt}	A_{xs} at T_{coll}	Absolute Error A_{xs} at T_{coll}	A_{uncorr} values used for A_{supp} calculation and A_{supp}
KC3B	1	2.00	0.15	0.88	0.28	
KC3B	5	1.64	0.15	0.51	0.28	
KC3B	9	1.47	0.14	0.33	0.27	
KC3B	14	1.43	0.13	0.29	0.26	
KC3B	19	1.68	0.15	0.55	0.28	
KC3B	24	2.33	0.20	1.22	0.33	
KC3B	29	1.22	0.13	0.07	0.25	*****1.22
KC3B	34	1.07	0.12	-0.07	0.25	*****1.07
						$A_{\text{supp}} = 1.14$
KC3C	1	13.03	0.91	11.40	1.05	
KC3C	3	14.36	1.15	12.69	1.29	
KC3C	7	13.65	0.97	12.04	1.11	
KC3C	14	12.52	1.00	10.83	1.13	
KC3C	19	11.35	0.81	9.70	0.94	
KC3C	24	9.82	0.77	8.10	0.90	
KC3C	29	2.29	0.17	0.48	0.30	
KC3C	34	1.67	0.14	-0.15	0.26	*****1.67
KC3C	44	1.84	0.15	0.03	0.27	*****1.84
KC3C	56	1.80	0.15	-0.02	0.27	*****1.80
KC3C	70	1.81	0.15	0.00	0.27	*****1.81
KC3C	84	1.97	0.16	0.16	0.29	*****1.97
KC3C	98	1.89	0.15	0.08	0.28	*****1.89
KC3C	110	1.71	0.15	-0.10	0.27	*****1.71
						$A_{\text{supp}} = 1.81$
KC3D	1	8.08	0.59	7.28	0.72	
KC3D	3	7.17	0.53	6.32	0.66	
KC3D	5	5.20	0.40	4.35	0.53	
KC3D	14	6.86	0.50	6.01	0.63	
KC3D	24	5.16	0.38	4.28	0.51	
KC3D	29	3.56	0.26	2.68	0.39	
KC3D	34	2.72	0.20	1.82	0.33	
KC3D	44	2.06	0.17	1.16	0.29	
KC3D	56	1.65	0.13	0.73	0.26	
KC3D	70	1.03	0.09	0.11	0.21	*****1.03
KC3D	84	0.99	0.09	0.07	0.21	*****.99
KC3D	98	0.73	0.06	-0.20	0.19	*****.73
KC3D	122	0.94	0.09	0.02	0.21	*****.94
						$A_{\text{supp}} = .92$

Station	Midpoint	A_{uncorr} at T_{plt}	Absolute Error A_{uncorr} at T_{plt}	A_{xs} at T_{coll}	Absolute Error A_{xs} at T_{coll}	A_{uncorr} values used for A_{supp} calculation and A_{supp}
KC3E	1	11.69	0.84	10.85	0.97	
KC3E	5	12.73	0.96	11.91	1.10	
KC3E	14	10.34	0.80	9.44	0.94	
KC3E	24	10.24	0.73	9.34	0.86	
KC3E	34	5.24	0.45	4.28	0.58	
KC3E	44	4.85	0.37	3.89	0.50	
KC3E	56	2.43	0.19	1.44	0.32	
KC3E	70	1.84	0.15	0.84	0.27	
KC3E	84	1.43	0.11	0.42	0.24	
KC3E	98	1.21	0.10	0.20	0.23	
KC3E	110	1.04	0.09	0.03	0.21	*****1.04
KC3E	122	1.03	0.09	0.02	0.21	*****1.03
KC3E	134	0.97	0.08	-0.04	0.20	*****.97
						$A_{\text{supp}} = 1.01$
KC3F	1	12.99	0.91	11.39	1.05	
KC3F	3	13.70	0.97	12.07	1.10	
KC3F	9	10.70	0.76	9.07	0.89	
KC3F	14	10.40	0.76	8.72	0.89	
KC3F	19	8.78	0.63	7.12	0.76	
KC3F	24	3.20	0.23	1.44	0.36	
KC3F	34	1.95	0.15	0.18	0.28	
KC3F	44	1.81	0.14	0.04	0.27	*****1.81
KC3F	56	1.71	0.15	-0.06	0.27	*****1.71
KC3F	70	1.74	0.13	-0.04	0.26	*****1.74
KC3F	84	1.74	0.14	-0.04	0.26	*****1.74
KC3F	98	1.82	0.15	0.05	0.28	*****1.82
KC3F	110	1.82	0.15	0.05	0.27	*****1.82
						$A_{\text{supp}} = 1.77$
KC3G	1	31.45	2.28	30.73	2.44	
KC3G	3	23.38	1.70	22.48	1.85	
KC3G	14	17.71	1.35	16.72	1.49	
KC3G	24	15.20	1.11	14.17	1.25	
KC3G	34	8.13	0.58	7.00	0.71	
KC3G	39	10.34	0.73	9.26	0.87	
KC3G	44	2.33	0.20	1.11	0.32	
KC3G	56	2.08	0.16	0.86	0.29	
KC3G	70	2.17	0.18	0.95	0.30	
KC3G	84	2.46	0.19	1.24	0.32	
KC3G	98	1.92	0.15	0.69	0.28	
KC3G	110	1.49	0.12	0.26	0.25	
KC3G	122	1.20	0.10	-0.04	0.23	*****1.20
KC3G	134	1.28	0.11	0.04	0.24	*****1.28
						$A_{\text{supp}} = 1.24$

**TRAN-
SECT 4**

Station	Midpoint	A_{uncorr} at T_{plt}	Absolute Error A_{uncorr} at T_{plt}	A_{xs} at T_{coll}	Absolute Error A_{xs} at T_{coll}	A_{uncorr} values used for A_{supp} calculation and A_{supp}
KC4A	1	11.02	0.78	10.29	0.92	
KC4A	3	11.37	1.01	10.60	1.14	
KC4A	14	8.30	0.63	7.48	0.76	
KC4A	24	3.64	0.31	2.77	0.43	
KC4A	34	4.16	0.38	3.30	0.51	
KC4A	44	5.08	0.39	4.23	0.51	
KC4A	63	3.41	0.27	2.54	0.39	
KC4A	77	1.96	0.17	1.08	0.29	
KC4A	91	1.81	0.17	0.92	0.29	
KC4A	110	1.37	0.13	0.48	0.25	
KC4A	122	1.11	0.10	0.22	0.23	
KC4A	134	0.83	0.07	-0.07	0.20	*****.83
KC4A	146	0.89	0.08	0.00	0.21	*****.89
KC4A	158	0.96	0.09	0.07	0.21	*****.96
						$A_{\text{supp}} = .89$
KC4C	3	4.02	0.29	2.34	0.42	
KC4C	9	6.18	0.48	4.55	0.61	
KC4C	14	6.07	0.43	4.41	0.56	
KC4C	19	2.91	0.22	1.22	0.35	
KC4C	24	0.63	0.05	0.01	0.17	
KC4C	34	2.04	0.16	0.34	0.29	
KC4C	44	2.17	0.18	0.47	0.30	
KC4C	56	3.23	0.25	1.54	0.37	
KC4C	70	4.79	0.36	3.12	0.48	
KC4C	84	2.04	0.16	0.34	0.28	
KC4C	98	5.19	0.46	3.52	0.59	
KC4C	110	3.90	0.29	2.22	0.42	
KC4C	122	1.97	0.16	0.27	0.28	
KC4C	134	1.57	0.13	-0.14	0.25	*****1.57
KC4C	146	1.63	0.15	-0.07	0.28	*****1.63
KC4C	158	1.69	0.14	-0.02	0.27	*****1.69
KC4C	170	2.07	0.18	0.37	0.31	*****2.07
KC4C	182	1.55	0.14	-0.16	0.27	*****1.55
KC4C	194	1.34	0.12	-0.38	0.24	*****1.34
KC4C	206	1.96	0.16	0.26	0.29	*****1.96
KC4C	218	2.10	0.16	0.40	0.29	*****2.10
KC4C	230	1.46	0.12	-0.25	0.25	*****1.46
						$A_{\text{supp}} = 1.71$

Station	Midpoint	A_{uncorr} at T_{plt}	Absolute Error A_{uncorr} at T_{plt}	A_{xs} at T_{coll}	Absolute Error A_{xs} at T_{coll}	A_{uncorr} values used for A_{supp} calculation and A_{supp}
KC4D	1	15.57	1.09	14.92	1.23	
KC4D	3	15.25	1.07	14.53	1.20	
KC4D	9	8.21	0.61	7.45	0.74	
KC4D	14	4.42	0.33	3.58	0.46	
KC4D	24	1.90	0.15	1.03	0.27	
KC4D	34	6.36	0.45	5.54	0.58	
KC4D	44	5.79	0.47	4.96	0.60	
KC4D	56	4.49	0.34	3.65	0.47	
KC4D	70	3.71	0.31	2.86	0.43	
KC4D	84	2.11	0.16	1.24	0.29	
KC4D	98	1.25	0.10	0.36	0.23	
KC4D	110	1.38	0.12	0.50	0.25	
KC4D	122	1.77	0.15	0.90	0.27	
KC4D	134	1.53	0.13	0.66	0.26	
KC4D	146	1.22	0.10	0.34	0.23	
KC4D	158	0.94	0.08	0.05	0.20	****.94
KC4D	170	0.88	0.08	-0.01	0.21	****.88
KC4D	182	0.83	0.07	-0.06	0.19	****.83
KC4D	194	0.91	0.08	0.02	0.20	****.91
						$A_{\text{supp}} = .89$
KC4E	3	19.43	1.34	18.28	1.48	
KC4E	7	5.77	0.42	4.44	0.55	
KC4E	14	7.76	0.56	6.45	0.69	
KC4E	24	6.46	0.48	5.12	0.60	
KC4E	34	6.06	0.45	4.72	0.57	
KC4E	44	2.57	0.22	1.18	0.34	
KC4E	49	4.43	0.34	3.07	0.47	
KC4E	56	2.10	0.18	0.70	0.31	
KC4E	70	3.73	0.31	2.35	0.44	
KC4E	84	2.28	0.19	0.89	0.32	
KC4E	98	1.67	0.15	0.27	0.28	
KC4E	110	1.50	0.13	0.10	0.26	****1.50
KC4E	110	1.42	0.12	0.01	0.24	****1.42
KC4E	122	1.33	0.11	-0.08	0.23	****1.33
KC4E	134	1.50	0.13	0.09	0.25	****1.50
KC4E	146	1.29	0.11	-0.12	0.24	****1.29
						$A_{\text{supp}} = 1.41$

APPENDIX D

Kasten and Box Core Carbon Data: $\delta^{13}\text{C}$, Carbon, and Nitrogen**Box Cores**

Core name	depth (cm)	Weight (mg)	$\mu\text{g N}$	μgC	$\delta^{13}\text{C}$
BC1A	0.5	36.151	12.1	96.4	-23.90
BC1C	0.5	49.729	11.1	85.9	-24.08
BC1D	0.5	37.562	11.3	89.7	-24.26
BC1E	0.5	39.589	11.0	87.7	-24.12
BC1H	0.5	44.102	7.2	51.6	-23.78
BC2A	0.5	34.742	13.1	98.8	-24.38
BC2B	0.5	41.761	14.5	104.8	-24.01
BC2C	0.5	35.992	10.6	80.0	-23.95
BC3A	0.5	48.482	11.5	89.1	-24.07
BC3C	0.5	30.63	11.4	92.1	-23.93
BC3D	0.5	31.254	10.9	87.7	-24.09
BC3E	0.5	41.853	12.1	97.6	-24.10
BC3F	0.5	39.499	13.0	106.5	-24.37
BC4A	0.5	41.796	14.0	109.8	-23.50
BC4A	1.5	39.046	15.5	127.6	-23.55
BC4A	2.5	46.601	16.0	135.4	-23.75
BC4C	0.5	48.018	15.9	138.7	-24.92
BC4C	1.5	43.6	15.0	130.9	-24.35
BC4C	2.5	48.088	13.8	121.0	-24.20
BC4E	0.5	46.504	14.4	112.2	-24.18

Kasten Cores

Core name	depth (cm)	Weight (mg)	$\mu\text{g N}$	$\mu\text{g C}$	$\delta^{13}\text{C}$
KC3D	1	45.343	31.8	273.7	-24.64
KC3D	3	43.717	29.2	263.2	-24.77
KC3D	5	42.738	30.8	281.6	-25.04
KC3D	14	43.944	27.3	225.5	-23.81
KC3D	24	46.016	28.7	247.6	-23.84
KC3D	29	41.726	26.5	223.0	-23.82
KC3D	34	40.577	22.9	194.5	-23.88
KC3D	44	45.779	29.3	242.2	-23.76
KC3D	56	45.873	27.5	224.2	-23.63
KC3D	70	43.793	23.2	201.0	-23.49
KC3D	84	44.181	20.8	177.3	-22.88
KC3D	98	46.209	22.3	194.3	-23.54
KC4C	3	40.368	26.1	269.0	-25.14
KC4C	9	46.378	36.5	333.0	-25.14
KC4C	14	40.339	33.5	352.5	-25.78
KC4C	19	43.479	33.7	292.8	-26.47

Core name	depth (cm)	Weight (mg)	$\mu\text{g N}$	μgC	$\delta^{13}\text{C}$
KC4C	24	46.059	32.6	313.0	-26.05
KC4C	34	42.026	55.5	1018.8	-27.22
KC4C	44	43.382	68.1	1205.8	-27.24
KC4C	56	42.829	65.3	1188.7	-27.22
KC4C	84	42.854	39.8	467.0	-26.47
KC4C	98	45.198	35.0	395.8	-25.59
KC4C	110	41.427	31.0	280.7	-24.81
KC4C	122	44.189	38.3	397.8	-25.95
KC4C	134	44.253	53.6	717.4	-26.62
KC4C	146	40.337	34.4	326.2	-25.83
KC4C	158	43.405	35.9	384.8	-25.85
KC4C	170	43.255	32.8	313.6	-25.26
KC4C	182	42.121	41.1	500.2	-26.35
KC4C	194	45.551	44.8	724.1	-26.99

APPENDIX E

Kasten Core Grain Size Computations

Core	Interval	% sand	% silt	% clay
KC1D	56	17.09	38.22	44.69
KC1D	70	27.07	36.75	36.18
KC3D	1	8.87	52.59	38.54
KC3D	3	7.83	49.79	42.38
KC3D	5	4.82	47.82	47.37
KC3D	7	2.69	50.78	46.53
KC3D	9	2.94	52.89	44.17
KC3D	14	13.52	39.79	46.70
KC3D	19	13.78	53.52	32.69
KC3D	24	14.93	51.23	33.84
KC3D	34	16.66	51.86	31.48
KC3D	39	16.76	52.46	30.79
KC3D	44	16.58	50.66	32.76
KC3D	49	22.77	47.30	29.93
KC3D	56	25.84	47.56	26.61
KC3D	63	32.24	46.58	21.19
KC3D	70	27.77	48.01	24.22
KC3D	77	44.30	37.03	18.67
KC3D	84	39.23	41.68	19.08
KC4A	24	3.61	38.38	58.02
KC4A	44	4.26	34.86	60.88
KC4C	3	1.62	42.74	55.64
KC4C	5	1.61	45.68	52.70
KC4C	7	3.97	41.26	54.76
KC4C	9	2.42	23.59	73.99
KC4C	14	5.69	50.35	43.95
KC4C	19	13.03	26.79	60.18
KC4C	24	0.58	21.87	77.55
KC4C	29	6.22	52.34	41.44
KC4C	39	9.15	53.91	36.95
KC4C	44	14.54	56.13	29.33
KC4C	49	11.18	56.96	31.86
KC4C	51	12.85	58.84	28.31
KC4C	56	11.92	57.73	30.34
KC4C	63	15.83	52.76	31.41
KC4C	70	24.12	36.01	39.87

Core	Interval	% sand	% silt	% clay
KC4C	77	1.61	27.39	71.00
KC4C	84	1.09	19.21	79.70
KC4C	91	9.75	55.43	34.82
KC4C	98	18.44	31.99	49.57
KC4C	110	5.28	35.35	59.38
KC4C	122	3.55	39.47	56.98
KC4C	134	7.44	43.36	49.20
KC4C	158	2.97	50.28	46.75
KC4C	170	5.34	35.33	59.32
KC4C	182	4.55	49.88	45.57
KC4C	194	9.02	65.47	25.52
KC4C	206	5.95	39.92	54.13
KC4C	218	4.11	36.34	59.56
KC4C	230	2.75	40.95	56.30
KC4D	1	6.16	35.57	58.26
KC4D	24	1.89	51.31	46.79
KC4D	98	1.86	57.27	40.87
KC4D	122	3.51	37.01	59.48
KC4E	44	0.64	31.80	67.56
KC4E	56	1.85	32.32	65.84
KC4E	70	6.90	35.29	57.81

REFERENCES

- Alexander, C.R., Venherm, C., 2003. Modern sedimentary processes in the Santa Monica, California continental margin: sediment accumulation, mixing and budget. *Marine Environmental Research*, 56, 177-204.
- Appleby, P.G., Oldfield, F., 1978. The calculation of ^{210}Pb dates assuming a constant rate of supply of unsupported ^{210}Pb to the sediment, 1-8. In Ivanovich, M., Harmon, R.S. (Eds.), *U-series Disequilibrium: Applications to Earth, Marine, and Environmental Sciences* (pp. ?). Oxford Science Publications.
- Benninger, L.K., Aller, R.C., Cochran, J.K., Turekian, K.K., 1979. Effects of biological sediment mixing on the ^{210}Pb chronology and trace metal distribution in a Long Island Sound sediment core. *Earth and Planetary Science Letters*, 43, 2, 241-259.
- Berdeal, I.G., Hickey, B.M., Kawase, M., 2002. Influence of wind stress and ambient flow on a high discharge river plume. *Journal of Geophysical Research*, 107, C9, 3130.
- Carter, L., Carter, R.M., McCave, I.N., Gamble, J., 1996. Regional sediment recycling in the abyssal Southwest Pacific Ocean. *Geology*, 24, 8, 735-738.
- Chiswell, S.M., 2000. The Wairarapa Coastal Current. *New Zealand Journal of Marine and Freshwater Research*, 34, 303-315.
- Collot, J.Y., Lewis, K., Lamarche, G., Lallemand, S. 2001. The giant Ruatoria debris avalanche on the northern Hikurangi margin, New Zealand: Result of oblique seamount subduction. *Journal of Geophysical Research*, 106, B9, 19271-19297.
- Davies, A.M., Xing, J., 2002. Processes influencing suspended sediment movement on the Malin–Hebrides shelf. *Continental Shelf Research*, 22, 15, 2081-2113.
- Farnsworth, K.L., Milliman, J.D., 2003. Effects of climatic and anthropogenic change on small mountainous rivers: the Salinas River example. *Global and Planetary Change*, 39, 53-64.
- Gee, G.W., Bauder, J.W., 1986. Particle-size analysis. In: Klute, A. (Ed.), *Methods of Soil Analysis: Part 1. Physical and Mineralogical Methods*, 2nd edn., Agronomy, 9. Soil Science Society of America, Madison, USA, pp. 383–411.
- Geyer, W.R., Hill, P.S., Kineke, G.C., 2004. The transport, transformation, and dispersal of sediment by buoyant coastal flows. *Continental Shelf Research*, 24, 927-949.

- Geyer, W.R., Hill, P., Milligan, T., Traykovski, P., 2000. The structure of the Eel River plume during floods. *Continental Shelf Research*, 20, 16, 2067-2093.
- Giffin, D., Corbett, D.R., 2003. Evaluation of sediment dynamics in coastal systems via short-lived radioisotopes. *Journal of Marine Systems*, 42, 83-96.
- He, Q., Walling, D.E., 1995. Interpreting particle size effects in the adsorption of ^{137}Cs and unsupported ^{210}Pb by mineral soils and sediments. *Journal of Environmental Radioactivity*, 30, 2, 117-137.
- Hicks, D.M., Griffiths, G.A., 1992. Sediment Load. In: Mosley, MP (ed), *Waters of New Zealand*. Wellington North, NZ: N.Z. Hydrological Society.
- Hicks, M., Shankar, U., McKerchar, A., 2003. Sediment Yield Estimates: a GIS tool. *Water and Atmosphere*, 11, 4, 26-27.
- Kineke, G.C., Woolfe, K.J., Kuehl, S.A., Milliman, J.D., Dellapenna, T.M., Purdon, R.G., 2000. Sediment export from the Sepik River, Papua New Guinea: evidence for a divergent sediment plume. *Continental Shelf Research*, 20, 2239-2266.
- Kranck, K., Milligan, T., 1991. Grain size in oceanography. In: Syvitski, J.P.M. (Ed.), *Principles, Methods, and Application of Particle Size Analysis*. Cambridge University Press, Cambridge, pp. 332-345.
- Leithold, E.L., Hope, R.S., 1999. Deposition and modification of a flood layer on the northern California shelf: lessons from and about the fate of terrestrial particulate organic carbon. *Marine Geology*, 154, 1-4, 183-195.
- Lewis, K.B., Barnes, P.M., 1999. Kaikoura Canyon, New Zealand: active conduit from near-shore sediment zones to trench-axis channel. *Marine Geology*, 162, 39-69.
- Lewis, R.C., Coale, K.H., Edwards, B.D., Marot, M., Douglas, J.N., Burton, E.J., 2002. Accumulation rate and mixing of shelf sediments in the Monterey Bay National Marine Sanctuary. *Marine Geology*, 181, 157-169.
- Milliman, J.D., Meade, R.H., 1983. World-wide delivery of river sediment to the oceans. *Journal of Geology*, 91, 1-21.
- Milliman, J.D., Syvitski, J.P.M., 1992. Geomorphic/Tectonic control of sediment discharge to the Ocean: The importance of small mountainous rivers. *Journal of Geology*, 100, 525-544.
- Mulder, T., Syvitski, J.P.M., 1995. Turbidity currents generated at river mouths during exceptional discharges to the world oceans. *Journal of Geology*, 103, 285-299.

Mulder, T., Syvitski, J.P.M., Migeon, S., Faugeres, J.C., Savoye, B., 2003. Marine hyperpycnal flows: initiation, behavior, and related deposits. A review. *Marine and Petroleum Geology*, 20, 861-882.

Mulder, T., Savoye, B., Piper, D.J.W., Syvitski, J.P.M., 1998a. The Var submarine sedimentary system: understanding Holocene sediment delivery processes and their importance to the geological record. In M.S. Stocker, D. Evans & A. Cramp (Eds.), *Geological processes on continental margins: sedimentation, mass-wasting and stability* (pp. 145-166). Geological Society of London, Special Publication, 129.

Mullenbach, B.L., Nittrouer, C.A., 2000. Rapid deposition of fluvial sediment in the Eel Canyon, Northern California. *Continental Shelf Research*, 20, 2191-2212.

Nittrouer, C.A., Sternberg, R.W., Carpenter, R., Bennett, J.T., 1979. The use of Pb-210 geochronology as a sedimentological tool: application to the Washington continental shelf. *Marine Geology*, 31, 297-316.

Page, M., Harmsworth, G., Trustrum, N., Kasai, M., Marutani, T., 2001. Waiapu River pg 102-111, in: Marutani, Tomomi, Gary J. Brierley, Noel A. Trustrum, and Mike Page (eds). *Source-to-Sink Sedimentary Cascades in Pacific Rim Geo-Systems*. Matsumoto Sabo Work Office, Ministry of Land, Infrastructure and Transport, Nagano, Japan. 184 p.

Parsons, J.D., Bush, J., Syvitski, J.P.M., 2001. Hyperpycnal flow formation with small sediment concentrations. *Sedimentology*, 48, 465-478.

Pickrill, R.A. and Mitchell, J.S., 1979. Ocean wave characteristics around New Zealand. *New Zealand Journal of Marine & Freshwater Research*, 13, 4, 501-520.

Scully, M.E., Friedrichs, C.T., Wright, L.D., 2002. Application of an analytical model of critically stratified gravity-driven sediment transport and deposition to observations from the Eel River continental shelf, Northern California. *Continental Shelf Research*, 22, 1951-1974.

Sommerfield, C.K., Nittrouer, C.A., Alexander, C.R., 1999. ^7Be as a tracer of flood sedimentation on the northern California continental margin. *Continental Shelf Research*, 19, 335-361.

Sommerfield, C.K., Nittrouer, C.A., 1999. Modern accumulation rates and a sediment budget for the Eel shelf: a flood-dominated depositional environment. *Marine Geology*, 154, 227-241.

Traykovski, P., Geyer, W.R., Irish, J.D., Lynch, J.F., 2000. The role of wave-induced density-driven fluid mud flows for cross-shelf transport on the Eel River continental shelf. *Continental Shelf Research*, 20, 16, 2113-2140.

Tsumune, D., Aoyama, M., Hirose, K., 2003. Numerical simulation of ^{137}Cs and $^{239, 240}\text{Pu}$ concentrations by an ocean general circulation model. *Journal of Environmental Radioactivity*, 69, 61-84.

Walcott, R.I., 1987. Geodetic strain and the deformational history of the North Island of New Zealand during the late Cainozoic. *Phil. Trans. R. Soc. Lond.* 321, 163-181.

Wright, L.D., 1977. Sediment transport and deposition at river mouths: a synthesis. *Geological Society of America Bulletin*, 88, 857-868.

Wright, L.D., Friedrichs, C.T., Kim, S.C., Scully, M.E., 2001. Effects of ambient currents and waves on gravity-driven sediment transport on continental shelves. *Marine Geology*, 175, 25-45.

Wright, L.D., Ma, Y., Scully, M., Friedrichs, C.T., 2005. Observations of storm driven benthic flows on the continental shelf off the Waiapu River, New Zealand. *Margins Conference*, Wellington, New Zealand.